Geophys. J. Int. (2009) **179,** 972–989 doi: 10.1111/j.1365-246X.2009.04330.x

Modelling flow in a pressure-sensitive, heterogeneous medium

D. W. Vasco[1] and Susan E. Minkoff[2]

[1] *Berkeley Laboratory, University of California, Berkeley,* CA 94720*, USA. E-mail: dwvasco@lbl.gov*
[2] *University of Maryland Baltimore County, Department of Mathematics and Statistics,* 1000 *Hilltop Circle, Baltimore,* MD 21250, USA

Accepted 2009 July 8. Received 2009 July 8; in original form 2008 December 12

GJI Marine geosciences and applied geophysics

SUMMARY

Using an asymptotic methodology, including an expansion in inverse powers of $\sqrt{\omega}$, where ω is the frequency, we derive a solution for flow in a medium with pressure dependent properties. The solution is valid for a heterogeneous medium with smoothly varying properties. That is, the scale length of the heterogeneity must be significantly larger then the scale length over which the pressure increases from it initial value to its peak value. The solution is in the form of a travelling disturbance and is defined along a trajectory through the medium, similar to a ray. The expression for pseudo-phase, which is related to the 'traveltime' of the transient pressure disturbance, and the expression for pressure amplitude contain modifications due to the pressure dependence of the medium. We apply the method to synthetic and observed pressure variations in a deforming medium. In the synthetic test we model 1-D propagation in a pressure-dependent medium. Comparisons with both an analytic self-similar solution and the results of a numerical simulation indicate general agreement. Furthermore, we are able to match pressure variations observed during a pulse test at the Coaraze Laboratory site in France.

Key words: Non-linear differential equations; Transient deformation; Geomechanics; Hydrology; Permeability and porosity; Wave propagation.

1 INTRODUCTION

The introduction of a volume of fluid into the Earth will induce some degree of deformation within the geological material comprising the subsurface. In most cases the resulting deformation is not significant, or even observable, and may be safely ignored. However, in some situations, such as poorly consolidated sediments, fractured media (Gale 1975; Jones 1975; Noorishad *et al.* 1992; Cappa *et al.* 2008) and large pressure changes and flow rates (Fatt 1958; Raghavan *et al.* 1972; Rutqvist *et al.* 1998), the changes within the matrix may impact the flow in important ways. For example, large pressure changes can modify the flow properties such as porosity and permeability, rendering the problem non-linear. Also, due to the transmission of stress within the medium, pressure changes can lead to non-local effects.

A comprehensive approach to this problem involves coupled modelling of the fluid flow and the deformation. Such coupled modelling can be complicated, making numerical methods attractive. While the utility of numerical modelling is well established (Noorishad *et al.* 1992; Rutqvist *et al.* 2002; Minkoff *et al.* 2003, 2004; Dean *et al.* 2006), analytic solutions can aid in our understanding, providing explicit relationships between medium parameters and properties of the pressure and deformation. Thus, analytic solutions can provide insight, complementing existing numerical approaches. To date, analytic studies of the coupled problem have been restricted to relatively simple cases, such as a homogeneous medium in which the flow properties do not change as a function of pressure. A classic example is a homogeneous poroelastic medium (Booker & Carter 1986; Rudnicki 1986) which can exhibit the non-local effects noted above (Segall 1985). Recently, a semi-analytic solution was developed for a poroelastic medium with heterogeneous flow properties which also contained non-local effects due to the coupling of the diffusive Biot wave and the 'fast' elastic wave (Vasco 2008, 2009). While coupled modelling provides a more complete and satisfactory approach for understanding flow in a deformable medium, it is also useful to examine particular aspects of this problem. In this paper, we examine the situation in which the flow properties are functions of the fluid pressure and we neglect the transmission of elastic deformation throughout the medium. As such, this paper complements studies which concentrate on the coupled problem, neglecting pressure dependent flow properties.

Allowing for pressure dependent flow properties leads to a non-linear diffusion equation (Wu & Pruess 2000). The non-linear diffusion equation has been used to model the flow of fluids in a deformable medium (Barenblatt 1952), flow in rock joints with pressure-dependent openings (Murphy *et al.* 2004), temperature and pressure waves in fluid saturated rock (Natale & Salusti 1996), and compaction in sedimentary basins (Audet & Fowler 1992) among other things (Newman 1983). The non-linear diffusion equation has been studied rather extensively from a mathematical perspective (Crank 1975; Hayashi *et al.* 2006), particularly for a homogeneous medium and for the case in which the permeability is proportional to the pressure raised to a power. In this instance one may derive an exact self-similar solution to the non-linear diffusion equation

(Boussinesq 1904; Leibenzon 1947; Polubarinova-Kochina 1948; Zel'dovich & Kompaneets 1950; Barenblatt 1952; Pattle 1959; Boyer 1961; Peletier 1971; Tuck 1976; Gilding & Peletier 1977; Pert 1977; Grundy 1979; Lacey *et al.* 1982; Matsuno 1991; King 1993; Korsunsky 1997). The 1-D self-similar solutions have also generalized to include heterogeneity in a special separable form (Kamin & Rosenau 1981; Grundy 1983). Asymptotic (Peletier 1970) and group-theoretic (Bluman & Cole 1974) methods have been used to consider a general dependence of the permeability on pressure, though only for a homogeneous medium.

In this paper, we derive a semi-analytic solution to the non-linear pressure equation. Because a goal of this work is to develop tools for solving the inverse problem, it is important that the solution be valid in the presence of 3-D, smoothly varying heterogeneity, and for a fairly general dependence on pressure, even an empirical laboratory-derived relationship. The solution is derived using an asymptotic technique (Jeffrey & Kawahara 1982; Anile *et al.* 1993), similar to ray-theoretical approaches used in modelling the propagation of elastic and electromagnetic waves, (Friedlander & Keller 1955; Kline & Kay 1965; Luneburg 1966; Kravtsov & Orlov 1990; Virieux *et al.* 1994), and transient pressure diffusion (Cohen & Lewis 1967; Vasco *et al.* 2000). As such, we will present expressions for the pressure pseudo-phase, which is related to the 'arrival time' of the transient disturbance, and for the pressure amplitude.

2 METHODOLOGY

2.1 The governing equation

Our starting point is the continuity equation for a fluid (Bear 1972, p. 197; de Marsily 1986, p. 85)

$$\nabla \cdot (\rho \mathbf{U}) + \frac{\partial}{\partial t}(\rho\phi) + q = 0, \tag{1}$$

where ρ is the fluid density, $\mathbf{U}$ is the fluid velocity vector, ϕ is the total porosity of the host material and q is the flow rate of fluid injected or withdrawn from the volume. Eq. (1) states that the rate of change in the fluid mass of an elemental volume equals the divergence of fluid from the volume and the rate at which fluid is injected or withdrawn from the volume. Augmenting this equation with Darcy's law which relates the fluid flow velocity vector, $\mathbf{U}(\mathbf{x}, t)$, to the gradient of the fluid pressure, $P(\mathbf{x}, t)$,

$$\mathbf{U} = -K\nabla P, \tag{2}$$

where the constant of proportionality, the normalized permeability K, depends upon the intrinsic or specific permeability k and the dynamic viscosity of the fluid μ

$$K = \frac{k}{\mu}. \tag{3}$$

Typically, when modelling fluid flow within the Earth it is assumed that the flow properties, in particular ϕ and K do not depend upon the fluid pressure. In this paper, we relax this assumption and allow ρ, ϕ and K to be functions of the fluid pressure. In addition, both ϕ and K are assumed to be functions of the spatial coordinates $\mathbf{x}$. Thus, we can write the porosity and permeability as the functions $\phi(\mathbf{x}, P)$ and $K(\mathbf{x}, P)$, respectively. In addition, we allow the fluid density to be a function of pressure $\rho = \rho(P)$, signifying that any spatial and temporal density dependence is through the pressure change and not due to explicit changes in the fluid properties, such as variations in salinity. Note that, because the pressure is a function of space and time, the flow properties contain an implicit dependence on these variables in addition to the explicit dependence on $\mathbf{x}$.

Substituting Darcy's law (2) into the conservation eq. (1), we arrive at the equation

$$\nabla \cdot (\rho K \nabla P) = \frac{\partial}{\partial t}(\rho\phi) + q. \tag{4}$$

Grouping terms and defining the coefficients

$$K_\rho = \rho(P)K(\mathbf{x}, P) \tag{5}$$

and

$$\phi_\rho = \rho(P)\phi(\mathbf{x}, P) \tag{6}$$

allows us to rewrite eq. (4) as

$$\nabla \cdot \left(K_\rho \nabla P\right) = \frac{\partial \phi_\rho}{\partial t} + q. \tag{7}$$

Because ϕ_ρ only depends on time through its dependence on $P(\mathbf{x}, t)$, we can apply the chain rule to arrive at

$$\nabla \cdot \left(K_\rho \nabla P\right) = C_\rho \frac{\partial P}{\partial t} + q, \tag{8}$$

where we have defined the pressure-dependent coefficient

$$C_\rho(\mathbf{x}, P) = \frac{\partial \phi_\rho(\mathbf{x}, P)}{\partial P}. \tag{9}$$

Expanding the spatial derivative on the left-hand side we have

$$\nabla K_\rho \cdot \nabla P + \frac{\partial K_\rho}{\partial P}\nabla P \cdot \nabla P + K_\rho \nabla \cdot \nabla P = C_\rho \frac{\partial P}{\partial t} + q, \tag{10}$$

and, after dividing through by K_ρ, we can define

$$\boldsymbol{\Upsilon}(\mathbf{x}, P) = \nabla \ln K_\rho \tag{11}$$

$$\lambda(\mathbf{x}, P) = \frac{\partial \ln K_\rho}{\partial P}, \tag{12}$$

$$\kappa(\mathbf{x}, P) = \frac{C_\rho}{K_\rho}, \tag{13}$$

$$Q = \frac{q}{K_\rho}, \tag{14}$$

and then write eq. (10) as

$$\boldsymbol{\Upsilon} \cdot \nabla P + \lambda \nabla P \cdot \nabla P + \nabla \cdot \nabla P = \kappa \frac{\partial P}{\partial t} + Q \tag{15}$$

the governing equation for flow in a medium with pressure-sensitive properties. In eq. (15), we have included the source Q explicitly in the formulation. It is also possible to include the source as a boundary conditions which is incorporated into the solution of the homogeneous equation

$$\boldsymbol{\Upsilon} \cdot \nabla P + \lambda \nabla P \cdot \nabla P + \nabla \cdot \nabla P = \kappa \frac{\partial P}{\partial t}. \tag{16}$$

In some cases it may be more advantageous to follow this approach, and we mention it as one option for flow modelling. Note that both eqs (15) and (16) contain coefficients which depend upon both the pressure field, P, and upon spatial coordinates, $\mathbf{x}$. As such, they cannot be solve analytically, and one must resort to approximations in order to make progress. Our primary assumption will be that the

heterogeneity is smoothly varying, in a sense made precise in the next subsection and in Appendix A.

2.2 An asymptotic solution for flow in a medium with smoothly varying properties

One of the applications of this work will be to solve the inverse problem, in which flow properties are estimated from a set of observations. In most inverse problems one has a limited and sparsely distributed set of data and wishes to estimate a spatial distribution of properties, such as permeability. Thus, one does not have enough data to constrain the small-scale heterogeneity and typically seeks a smooth model which satisfies the data (Vasco *et al.* 2000). For this reason, we shall derive a solution which is valid in a medium with smoothly varying properties. Note that, though the heterogeneity is smooth overall, we can include a finite number of discontinuities, such as layering and faults, as boundaries in the model. That is, we can include explicit boundary conditions in which there are discontinuities in the flow properties, as is done in ray methods in optics, electromagnetics, elastic and poroelastic wave propagation (Luneburg 1966; Kline & Kay 1965; Kravtsov & Orlov 1990; Vasco 2008).

The exact definition of smooth is relative to the length scale over which the pressure changes from the background value to a new value induced by the pumping. Let us denote this length scale by l, and the length scale of the heterogeneity by L. Defining the ratio $\varepsilon = l/L$, and assuming that $\varepsilon \ll 1$, we can define new 'slow' space and time coordinates in terms of ε

$$X_i = \varepsilon x_i \tag{17}$$

and

$$T = \varepsilon^2 t. \tag{18}$$

The difference in scaling between the spatial variables and the temporal variables is necessary because we are considering a diffusive process and the order of the equation is different for the classes of variables. As shown in Appendix A, we can represent the solution as a power series in ε

$$P(\mathbf{X}, T) = P_0(\mathbf{X}) + \sum_{l=1}^{\infty} \varepsilon^l P_l(\mathbf{X}, T), \tag{19}$$

where $P_0(\mathbf{X})$ is the background pressure which is assumed to only vary in space. Because ε is small the lower order terms are the most important. Furthermore, because $\boldsymbol{\Upsilon}(\mathbf{X}, P)$, $\lambda(\mathbf{X}, P)$ and $\kappa(\mathbf{X}, P)$ are functions of P we can also expand them as power series in ε. Substituting the power series expansions into the governing equation (16) results in an equation containing an infinite number of terms, each of a specific order in ε,

$$\begin{aligned}\left[\boldsymbol{\Upsilon}(\mathbf{X}, P_0) + \sum_{l=1}^{\infty} \varepsilon^l \frac{\partial^l \boldsymbol{\Upsilon}}{\partial P^l} P_l(\mathbf{X}, T)\right] \cdot \nabla P \\ + \left[\lambda(\mathbf{X}, P_0) + \sum_{l=1}^{\infty} \varepsilon^l \frac{\partial^l \lambda}{\partial P^l} P_l(\mathbf{X}, T)\right] \nabla P \cdot \nabla P \\ + \nabla \cdot \nabla P = \left[\kappa(\mathbf{X}, P_0) + \sum_{l=1}^{\infty} \varepsilon^l \frac{\partial^l \kappa}{\partial P^l} P_l(\mathbf{X}, T)\right] \frac{\partial P}{\partial T}\end{aligned} \tag{20}$$

after factoring out ε^2 which multiplies each term (see Appendix A), which can be grouped according to their order in ε. In the next two subsections we consider terms of order ε^0 and ε^1.

2.3 Terms of order ε^0: an equation for $P_0(\mathbf{X})$

Because ε is assumed to be small, we am interested in terms of lowest order in ε. To the lowest order in ε we have an equation for $P_0(\mathbf{X})$, given by

$$\boldsymbol{\Upsilon}_0 \cdot \nabla P_0 + \lambda_0 \nabla P_0 \cdot \nabla P_0 + \nabla \cdot \nabla P_0 = 0, \tag{21}$$

where

$$\boldsymbol{\Upsilon}_0 = \boldsymbol{\Upsilon}(\mathbf{X}, P_0) \tag{22}$$

and

$$\lambda_0 = \lambda(\mathbf{X}, P_0). \tag{23}$$

Eq. (21) is a non-linear equation for the background pressure variation $P_0(\mathbf{X})$. For the most part, non-linear equations are difficult to solve and, with the possible exception of techniques from the theory of continuous groups (Bluman & Cole 1974; Olver 1986), there are no general methods that one can employ. Fortunately, the background pressure $P_0(\mathbf{X})$ only depends upon the spatial coordinates $\mathbf{X}$ and thus eq. (21) does not require time-stepping. Thus, numerical methods should allow for the efficient solution of the scalar eq. (21). Note that one possible solution to eq. (21) consists of a constant background pressure $P_0(\mathbf{X}) = P_b$.

2.4 Terms of order ε: a linear equation for $P_1(\mathbf{X}, T)$

Considering terms of order ε in eq. (20) results in a linear equation for $P_1(\mathbf{X}, T)$

$$\nabla \cdot \nabla P_1 + \boldsymbol{\Psi}_1 \cdot \nabla P_1 + \Psi_2 P_1 = \kappa_0 \frac{\partial P_1}{\partial T}, \tag{24}$$

where the coefficients depend on the medium parameters and the background pressure field,

$$\boldsymbol{\Psi}_1 = \boldsymbol{\Upsilon}_0 + 2\lambda_0 \nabla P_0, \tag{25}$$

$$\Psi_2 = \frac{\partial \boldsymbol{\Upsilon}_0}{\partial P} \cdot \nabla P_0 + \frac{\partial \lambda_0}{\partial P} \nabla P_0 \cdot \nabla P_0 \tag{26}$$

and

$$\kappa_0 = \kappa(\mathbf{X}, P_0) = \frac{C_\rho}{K_\rho},$$

where λ_0, $\partial\lambda_0/\partial P$, $\partial\Upsilon_0/\partial P$ and κ_0 are evaluated at $P = P_0(\mathbf{X})$. Even though eq. (24) is a linear diffusion equation, it is still not possible to solve it analytically. Such a solution is precluded by the presence of the coefficients $\boldsymbol{\Psi}_1$, Ψ_2 and κ_0 which depend upon $\mathbf{X}$.

Using the approach of Virieux *et al.* (1994) and following Vasco *et al.* (2000), we can derive a semi-analytic solution for $P_1(\mathbf{X}, T)$ which is valid for the high-frequency component of pressure. As discussed in Appendix B, the method is implemented in the frequency domain and requires the application of the Fourier transform to eq. (24)

$$\nabla \cdot \nabla \hat{P}_1 + \boldsymbol{\Psi}_1 \cdot \nabla \hat{P}_1 + \Psi_2 \hat{P}_1 = \mathrm{i}\omega\kappa_0 \hat{P}_1, \tag{27}$$

where $\hat{P}_1(\mathbf{X}, \omega)$ is the Fourier transform of $P_1(\mathbf{X}, T)$ (Bracewell 1978). In Appendix B an asymptotic solution for eq. (27) is derived, the zeroth-order term of the solution is

$$\hat{P}_1(\mathbf{X}, \omega) = A_0(\mathbf{X}) \mathrm{e}^{-\sqrt{-\mathrm{i}\omega}\sigma(\mathbf{X})} \tag{28}$$

which is characterized by an amplitude function $A_0(\mathbf{X})$ and a phase or 'pseudo-phase' function $\sigma(\mathbf{X})$. The phase function $\sigma(\mathbf{X})$ is a line integral along a trajectory $\mathbf{X}(s)$ through the model

$$\sigma(\mathbf{X}) = \int_{\mathbf{X}} \sqrt{\kappa_0} \mathrm{d}s \tag{29}$$

a function of the medium properties, as contained in κ_0. The expression of κ_0 in terms of the medium properties is given by eq. (13), evaluated at the background pressure P_0

$$\kappa_0 = \kappa(\mathbf{X}, P_0) = \frac{C_\rho(\mathbf{X}, P_0)}{K_\rho(\mathbf{X}, P_0)}. \tag{30}$$

The trajectory is the solution of a system of ordinary differential equations, as shown in Appendix B, eqs (B10) and (B11). Alternatively, as discussed in Vasco and Finsterle (2004), the trajectory can be computed by post-processing the output of a numerical simulator to derive the peak pressure arrival time and consequently, the phase $\sigma(\mathbf{X})$. In particular, the quantity $\sigma(\mathbf{X})$ is related to the time at which the peak pressure is observed, $T_{\rm peak}$. For an observation made at location $\mathbf{X}$, the exact relationship is $\sigma(\mathbf{X}) = \sqrt{6T_{\rm peak}}$. From the phase field one can compute the trajectories by numerically integrating eq. (B10), a much simpler approach than ray-tracing. Note that the integrand depends upon the flow properties due to the presence of κ_0. The amplitude function, $A_0(\mathbf{X})$, evolves along the trajectory according to

$$A_0(s) = A_0(s_0)\sqrt{\frac{K_x(s_0)}{K_x(s)}}\sqrt{\frac{\sqrt{\kappa_0(s_0)}J(s_0)}{\sqrt{\kappa_0(s)}J(s)}}\frac{\mathrm{e}^{-\eta(s_0)}}{\mathrm{e}^{-\eta(s)}}, \tag{31}$$

where $J(s)$ is the Jacobian which is a measure of the geometrical spreading of the trajectories as a function of distance (Kravtsov & Orlov 1990) and

$$\eta(s) = \int_0^s \lambda \frac{\mathrm{d}P_0}{\mathrm{d}\gamma'}\mathrm{d}\gamma'. \tag{32}$$

Applying the inverse Fourier transform to the expression (28) gives the time-domain equivalent

$$P_1(\mathbf{X}, T) = A_0(\mathbf{X})\sigma(\mathbf{X})\frac{\mathrm{e}^{-\sigma^2(\mathbf{X})/4T}}{2\sqrt{\pi T^3}} \tag{33}$$

which is similar in form to the solution of the diffusion equation for a homogeneous medium (de Marsily 1986, p. 162). However, the solution (33) accounts for smoothly varying heterogeneity in flow properties and pressure-sensitive flow properties.

We should note the special situations in which the source and medium are such that we may assume particular symmetries in the solution of eq. (24). For example, there may be problems in which we may consider a 1-D or 2-D solution. For a source and medium with m-dimensional radial symmetry the solution to the pressure equation is given by

$$P_1(\mathbf{X}, T) = A_0(\mathbf{X})\sigma(\mathbf{X})\frac{\mathrm{e}^{-\sigma^2(\mathbf{X})/4T}}{2\sqrt{\pi}T^{\frac{m+1}{2}}} \tag{34}$$

as noted by Virieux *et al.* (1994). Note that 0-D symmetry ($m = 0$) denotes a 1-D solution while 1-D and 2-D symmetry represent 2-D and 3-D solutions, respectively.

2.5 The full solution for pressure

The resulting expression for the pressure, valid to order ε, is obtained by combining the expressions for $P_0(\mathbf{X})$ and $P_1(\mathbf{X}, T)$

$$P(\mathbf{X}, T) = P_0(\mathbf{X}) + A_0(\mathbf{X})\sigma(\mathbf{X})\frac{\mathrm{e}^{-\sigma^2(\mathbf{X})/4T}}{2\sqrt{\pi T^3}}. \tag{35}$$

This expression is of the same form as the expression for pressure in a uniform medium (de Marsily 1986) and in a heterogeneous medium whose coefficients do not depend on pressure (Vasco *et al.* 2000). The form of the solution (35) is similar to the asymptotic solution of the non-linear heat equation discussed in Hayashi *et al.* (2006) though the assumptions of large $\mathbf{X}$ and T are not equivalent to those invoked in this paper. We should emphasize that eq. (35) is the impulse response: the pressure variation due to an impulsive source. For a general source one must convolve the impulse response with an appropriate source–time function (Vasco *et al.* 2000).

3 APPLICATIONS

3.1 Numerical illustrations

In this section, we implement the expressions for flow in a pressure-sensitive, heterogeneous medium. First, we compare the asymptotic solutions to an analytic self-similar solution and a numerical finite-element solution in a homogeneous medium in which the conductivity K only varies as a function of the pressure. Specifically, the conductivity is equal to the pressure to the power n. Next, we compare the self-similar and asymptotic solutions for a medium with cylindrical symmetry. Finally, we compare the asymptotic solution with a numerical result for a heterogeneous medium with pressure-sensitive permeability.

3.1.1 Comparison with analytic and numerical solutions

As noted in Section 1, in a medium in which the conductivity varies as the pressure to a power n,

$$K = P^n, \tag{36}$$

one can take advantage of the self-similarity of the problem to deduce an analytic solution as a function of spatial location (x) and time (t) (Boussinesq 1904; Leibenzon 1947; Polubarinova-Kochina 1948; Zel'dovich & Kompaneets 1950; Barenblatt 1952; Pattle 1959; Boyer 1961; Tuck 1976; Pert 1977; Grundy 1979; Lacey *et al.* 1982),

$$P(x, t) = \frac{1}{t^{1/(n+2)}}\left[\gamma - \frac{nx^2}{2(n+2)t^{2/(n+2)}}\right]^{1/n} \tag{37}$$

when $x < x_0$ and zero otherwise. The quantity γ is a constant of integration and x_0 is given by

$$x_0 = \sqrt{\frac{2(n+2)\gamma}{n}t^{2/(n+2)}}. \tag{38}$$

Here we compare the explicit solution presented in Tuck (1976) and given by eq. (37) with a numerical solution and with our asymptotic solution, eq. (35). A Galerkin finite element method is used to calculate the numerical solution to the pressure equation with pressure-sensitive coefficients (Minkoff & Kridler 2006).

We fix the density and the porosity at constant values for our comparison, that is, they are not sensitive to pressure variations. In this illustration, we consider the case in which $n = 0.5$, the source is an impulse, and the boundaries are open. Due to the specific form of the pressure-sensitive component of conductivity, eq. (36), we can derive an explicit expression for $\lambda(P)$, given by eq. (12),

$$\lambda(P) = \frac{\partial \ln K_p}{\partial P} = \frac{n}{P}. \tag{39}$$

The self-similar and asymptotic solutions appear to be very different in form and depend upon different parameters. For example, the self-similar solution depends on the constant of integration γ while the asymptotic solution depends on the background pressure P_0. We should point out that the pressure-dependence of K, given by

eq. (36) is a degenerate form. Specifically, for a general pressure dependence we expect a Taylor expansion of the form

$$K(P_0 + P) = K(P_0) + \frac{\partial K}{\partial P}|_{P_0} P + \frac{1}{2}\frac{\partial^2 K}{\partial^2 P}|_{P_0} P^2 + \cdots. \qquad (40)$$

For the relationship considered here, eq. (36), the lower order coefficients vanish and we are left with a single term. The asymptotic solution relies on the power series expansion of the coefficients (A9), (A10) and (A11) in which the partial derivatives are assumed to be non-zero. Thus, the functional form (36) represents a particularly difficult case for the asymptotic approach.

To compare the self-similar, numeric, and asymptotic solutions we calculated the pressure variations predicted by the three methods for observation points 100, 433, 767 and 1100 m away from the source (Fig. 1). In order to compare the results we normalized the pressure amplitudes such that the amplitudes at 500 s for the station 100 m from the source were unity. In general, the normalized pressures predicted by the three methods show good agreement (Fig. 1). Each set of curves displays the same relative amplitude for the four observation points. Furthermore, all the curves vary slowly in time after roughly 100 s. A more detailed comparison of the temporal variations for the observation point at 767 m from the source indicates the overall agreement between the three techniques (Fig. 2). There are some differences in detail between the predictions, but that is to be expected, given the variations in parametrizations and the various assumptions made in each approach. In order to examine the variations between the three methods we have plotted the relative and absolute errors or differences between the three solutions for an observation point at 767 m (Fig. 3). The top two panels display the differences between the asymptotic solution and the self-similar and numeric solutions, respectively. In general, the relative error is below 10 per cent except at early times when the values are close to zero and any difference is magnified significantly. The absolute error peaks at around 0.15 for the comparison with the self-similar solution and around 0.05 for the comparison with the numeric solution. Note that the difference between the asymptotic solution and the self-similar and numeric solutions is of the same order as the difference between the self-similar solution and the numeric solution. In fact, the discrepancy between the numeric and the asymptotic solutions is smaller than that between the numeric and the self-similar solutions. Thus, for this case the approximations leading to the asymptotic solution do not appear to introduce significant error.

3.1.2 Propagation in a medium with cylindrical symmetry

In this subsection, we consider a medium with cylindrical symmetry and the same properties as in the previous calculation. Here we compare the self-similar solution, given in Kamin & Rosenau (1981) to the asymptotic expression (34), with $m = 1$. Calculations were made for four distances from the source, 100, 433, 767 and 1100 m, as shown in Fig. 4. There is fair agreement between the two sets of pressure estimates with both methods indicating a rapid pressure decrease over time. This behaviour is predicted by the time dependence of the asymptotic solution, eq. (37), in which the solution decays as $1/T$ as compared to $1/\sqrt{T}$ in the previous example.

In Figs 5 and 6, three snapshots of the pressure variation are shown for the self-similar and asymptotic solutions, respectively. The pressure at each node point has been normalized by the peak value obtained at the node. Thus, the propagating pressure peaks

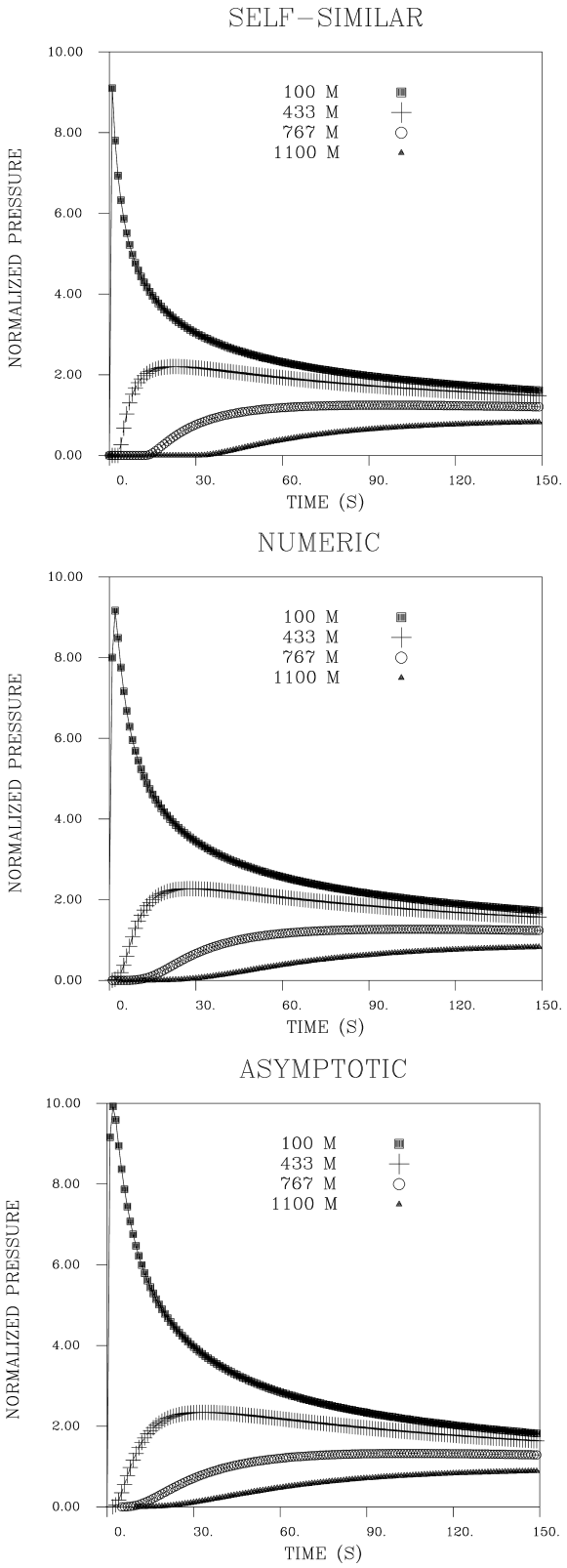

Figure 1. Pressure variations calculated using a self-similar, a numeric, and an asymptotic technique. The solutions correspond to a medium with a uniform initial conductivity and a pressure-dependence of the form $K = P^n$ where $n = 0.5$. The pressure-versus-time curves are plotted for four locations, 100, 433, 767 and 1100 m. The pressures have been normalized by the values at the 100 m location at a time of 500 s.

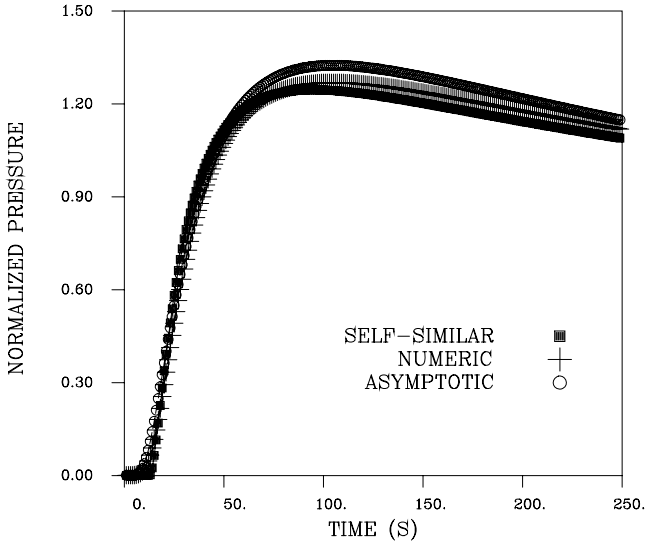

Figure 2. Detailed comparison of the self-similar, numeric, and asymptotic pressure estimates at a point 767 m from the source.

at values of one, and the pressure change at nodes further from the source are amplified relative to the pressure change near the source. With this scaling the pressure resembles a disturbance propagating away from the source, similar to a wave. Such transient propagation was noted for the linear heterogeneous pressure equation by Vasco & Finsterle (2004). In that study, in which the source was a step-function and not a delta-function, the pressure time derivative was plotted. There is overall agreement between the self-similar and the asymptotic solutions with differences in detail. For example, the self-similar solution seems to have a sharper outer boundary in comparison to the asymptotic solution. This is consistent with the fact that the self-similar solution is actually a generalized solution, with a discontinuity in the derivative at the leading edge of the pressure front (Peletier 1971).

3.1.3 Propagation in a heterogeneous medium

This application involves pressure propagation in a heterogeneous medium. The heterogeneity is in the form of a smoothly varying increase from a permeability of around 0.1 Darcies to just under 1.5 Darcies (Fig. 7). The increase is produced by the hyperbolic tangent function, $\tanh(x)$, with a width of 33 m. The full expression of the hydraulic conductivity is in a separable form

$$K(x, P) = K_x(x)K_p(P), \tag{41}$$

where $K_x(x)$ is the spatially varying component and $K_p(P)$ is the pressure dependent component. For comparison with our previous results, we consider a pressure dependent component of the form $K_p(P) = P^{1/2}$. The results, corresponding to a delta-function source at the origin, are shown in Fig. 8 for the numerical and asymptotic solutions. Due to the presence of the heterogeneity it was not possible to construct a self-similar analytic solution. Note the close correspondence of the two solutions at the four observation points, 10, 40, 70 and 100 m. There are some differences in the early time amplitude for the observation point at 10 m. However, the amplitude for this station, so close to the source, is likely to be sensitive to properties of the numerical simulation, such as the location of the finite element nodes.

3.2 Application to a hydromechanical pulse test conducted at the Coaraze Laboratory site, France

In this subsection, we analyse a pressure pulse test conducted at the Coaraze Laboratory field site in France, in which fluid is rapidly injected into a fracture (Cappa *et al.* 2006, 2008). We shall use the methods derived above to try and match the pressure changes recorded in an observation borehole. During the injection the fluid pressure and normal displacements are measured in two boreholes intersecting the fracture. Using a planar fracture model (Witherspoon *et al.* 1980) we can relate changes in flow properties to changes in pressure and to fracture deformation. Given these relationships we can use the expressions presented above to calculate the traveltime and amplitude variation due to propagation within the fracture.

3.2.1 The Coaraze Laboratory field site

The Coaraze Laboratory is located within the French Southern Alps and is a natural reservoir, 30 m × 30 m in areal extent, composed of a 15-m-thick sequence of dipping, fractured limestone bounded by impervious glauconous marl layers (Guglielmi & Mudry 2001). A 3-D model of the various fractures and bedding planes has been constructed, based upon surface exposures and borehole scan-line data (Cappa *et al.* 2006). There are two significant fracture sets, three near-vertical fractures trending northeast to east (North 50°–70° east) with a 2–3 m spacing, and eleven near-vertical fracture trending southeast (North 120°– 140° east) with a 2 m spacing. The permeability of the near-vertical fracture ranges from 0.6×10^{-4} to 1.9×10^{-4} m s^{-1}. In addition, there are 12 bedding planes, spaced 0.5–1.0 m within the limestone which trend north 40° east and dip roughly 45° towards the southeast. The permeability of the bedding planes is approximately two orders of magnitude less than that of the fractures, varying from 0.9×10^{-6} to 7.6×10^{-6} m s^{-1}. The limestone matrix is essentially impervious and, over the timescales considered, fluid storage and flow occurs within the fractures and bedding planes. A number of boreholes and surface sensors record deformation within the fractures and at the surface of the outcrop. In addition, pressure is measured in several boreholes intersecting the outcrop.

3.2.2 A pressure pulse test

The field experiment involved two horizontal boreholes (HM1 and HM2) intersecting one of the northeast trending subvertical fractures. The intersections of the wells with the fracture were isolated by inflatable packers to create a 0.4 m long sealed section. The borehole intersections were 1 m apart in the vertical direction. In each sealed section fiber-optic pressure and displacement sensors provided measurements of fluid pressure and fracture normal displacement as a function of time (Cappa *et al.* 2005, 2006). Pressure and displacement data were collected at 120 samples per second, a much higher rate than standard hydrologic pressure measurements, allowing for short-duration pulses and accurate timing (Cappa *et al.* 2008).

The pulse test involved injecting 1.2 l of water into borehole HM1 leading to a pulse of pressure of 86 kPa. The resulting pressure and normal displacements recorded in the two boreholes HM1 and HM2, are shown in Fig. 9. The total test duration is roughly 40 s, with the pulse beginning 15s after the start of monitoring. In the injection borehole HM1 the pressure increases rapidly, reaching a peak of around 125 kPa in less than 4 s (Cappa *et al.* 2005). The pressure decreases almost as rapidly though there is some slightly oscillatory

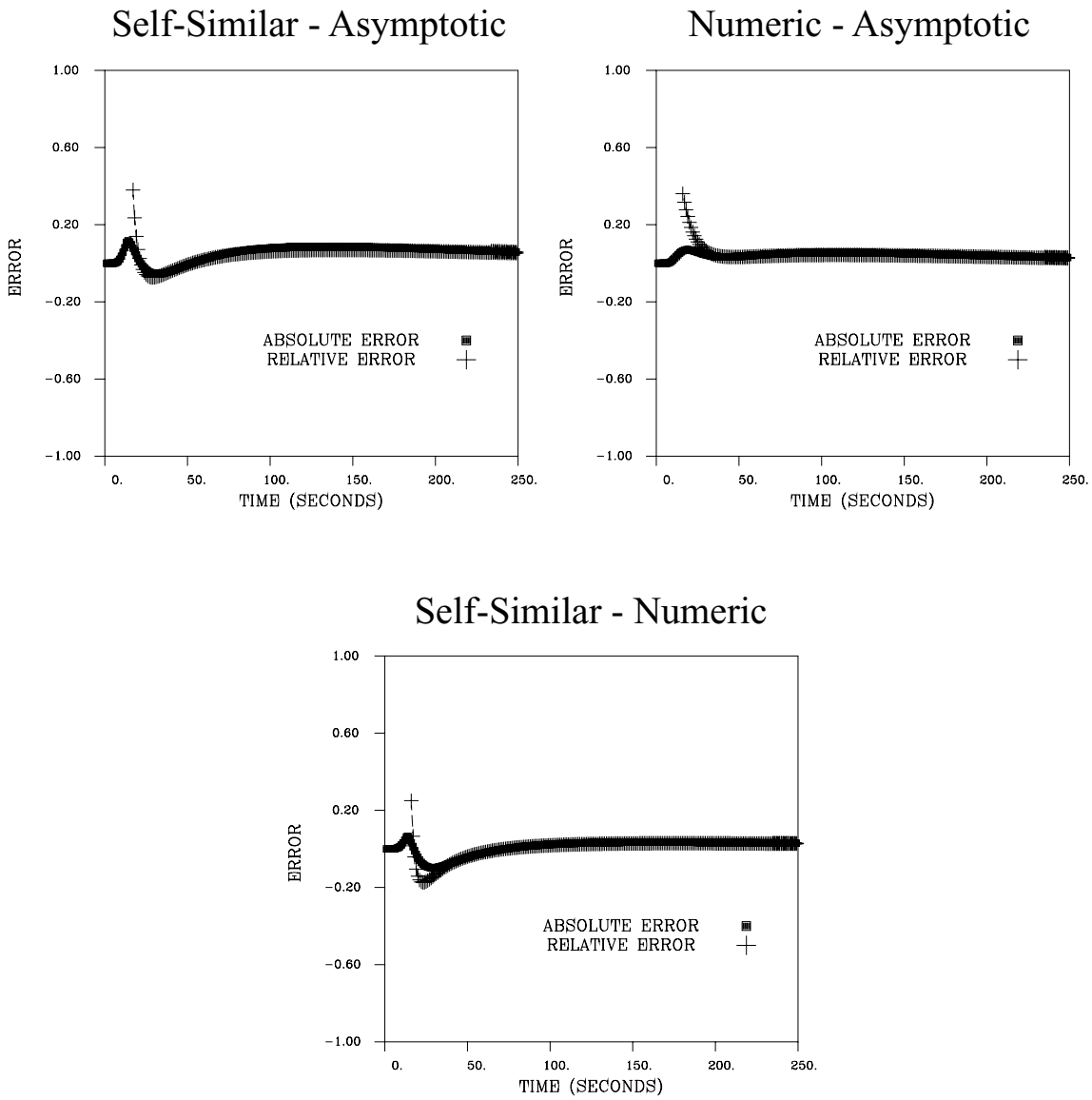

Figure 3. Relative and absolute differences between the various solutions. The relative error is given by the difference between the two solutions divided by the value of the first solution, relative error $= (f_2 - f_1)/f_1$, where f_1 is the first solution in the title. The absolute error is the straight-forward difference: $f_2 - f_1$.

behavior as it returns to the background value of 39 kPa, possibly due to inertial effects due to the high injection rate. The normal displacement observed at borehole HM1 is similar in nature to the pressure though the oscillations are muted and the decay back to the background value is slightly more gradual. In borehole HM2 the pressure increases from a background value of 27 kPa to a peak of 49 kPa, for a pressure change of 22 kPa. The pressure peak in borehole HM2 is delayed by 1.5 s with respect to the peak in the injection borehole HM1 (Cappa *et al.* 2008). The pulse shape has also changed significantly due to the 1 m of propagation within the fracture.

Normalizing the fracture displacement and plotting it on the same graph as the pressure reveals that, though both pulses start at the same time, the displacement quickly begins to lag the pressure (Fig. 10). The lag increases over time and is more pronounced in the tail of the pulses. The lag is most notable at the source borehole (HM1) and is not as clear at borehole HM2. The hysteresis is clearer if we plot pressure at a given time against the corresponding normal displacement (Fig. 11). The graph does not lie along a straight line, rather it forms a loop in which the arm of increasing pressure lies below that of decreasing pressure. Furthermore, in this type of plot the pressure lag at HM2 becomes clearer (Fig. 11) if we plot it at an appropriate scale. The hysteresis displayed in Fig. 11 has been noted by previous investigators (Cappa *et al.* 2006; Murdoch & Germanovich 2006).

Cappa *et al.* (2006) provide an explanation for the observed hysteresis in terms of the evolving pressure distribution within the fracture zone. In essence, the normal displacement of the fracture reflects the total pressure distribution within the fracture and not simply the local pressure field near the point of interest. Thus, the pressure increase 'props' open the fracture behind the propagating pressure front. Note that the non-linearity due to the pressure-dependent flow properties is an important part of this explanation. For example, the increase in permeability due to the opening

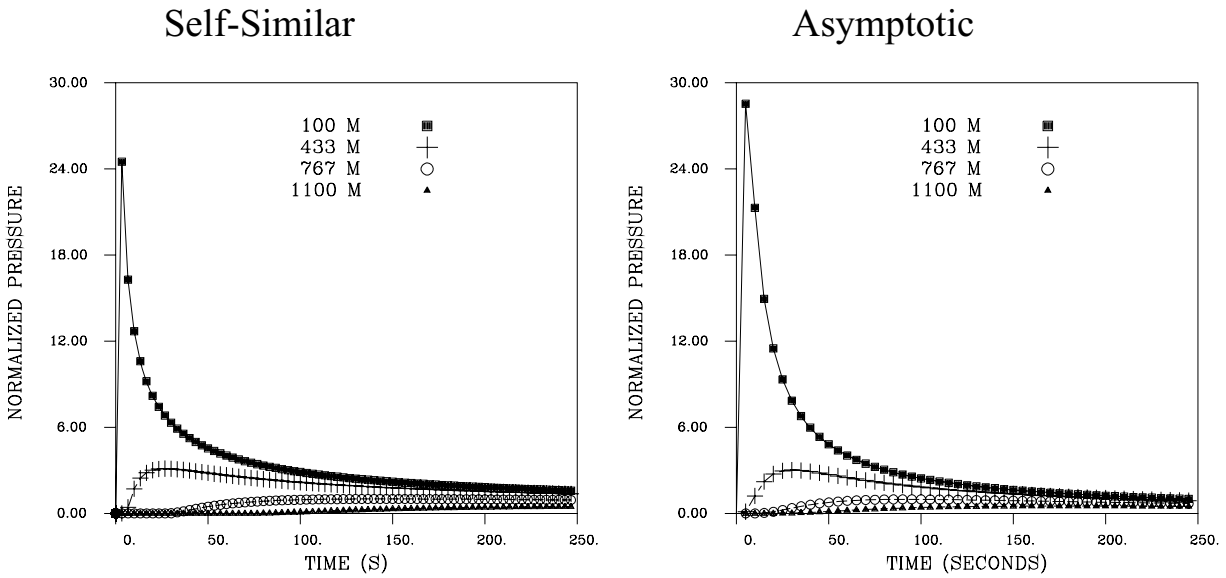

Figure 4. The self-similar and asymptotic solutions for a cylindrically symmetric medium. The medium properties are identical to the previous test case but the propagation is that of a cylindrical disturbance moving in the radial direction. The pressure variation is computed at four distances from the source: 100 m (filled squares), 433 m (crosses), 767 m (unfilled circles) and 1100 m (filled triangles).

fracture allows the pressure to equilibrate faster behind the propagating front. Furthermore, the pressure does not act at points ahead of the propagating pressure disturbance, where the permeability has not yet increased and is still at the lower background value. That is, the fracture does not open ahead of the arrival of the pressure pulse. In fact, the normal displacement recorded at HM2 indicates fracture closure ahead of the arrival of the pressure pulse. This may be due to a decrease in pressure, observed in borehole HM2 just before the arrival of the pressure pulse (Fig. 10).

3.2.3 Pressure dependent flow in a fracture

The deformation of the fracture due to the increase in fluid pressure changes its aperture and hence its flow properties. That is, as the fracture opens due to the pressure increase, its storage and permeability are altered. In this subsection, we derive expressions for pressure-sensitive permeability and storage for a simple fracture model.

Permeability

We begin with the analysis by Witherspoon *et al.* (1980), based upon earlier modelling of a fracture as two parallel plates (Boussinesq 1868; Lomize 1951; Romm 1966), which leads to the following law relating the fluid flow velocity vector **U** to the gradient in hydraulic head H (**x**, t)

$$\mathbf{U} = -\frac{(a_\mathrm{i} + f\Delta a)^2}{12}\frac{\rho g}{\mu}\nabla H, \tag{42}$$

where a_i is the initial aperture, f is a factor reflecting the influence of the fracture roughness, Δa is the change in aperture due to the pressure change, w is a geometrical factor related to the effective width of the fracture, ρ is the density of the fluid, g is the gravitational acceleration and μ is the dynamic viscosity of the fluid. The gradient in hydraulic head is related to the fluid pressure gradient according to the formula

$$\nabla H = \nabla\left(\frac{P}{\rho g} + z\right), \tag{43}$$

where z is the depth.

Assuming a constant fluid density we can write eq. (43) as

$$\nabla H = \frac{1}{\rho g}\nabla P + \mathbf{z}, \tag{44}$$

where **z** is the gradient vector in the direction of the z-axis. Note that if we integrate eq. (42) over the fracture aperture we arrive at the cubic law which relates flow within the fracture to the gradient of head within the fracture (Witherspoon *et al.* 1980).

The normal displacement of the fracture, Δa in eq. (42) is hypothesized to be due to changes in the effective stress field, $\bar{\sigma}_\mathrm{n}$, acting on the fracture. Terzaghi introduced the concept of effective stress to describe the stress that is transmitted between grains in a fluid saturated soil (Terzaghi 1923; Terzaghi & Peck 1967). For a fracture it is the stress transmitted from one side of the fracture to the other. As such, the normal stress σ_n is the stress that would be measured in the rock itself a short distance away from the fracture. The effective normal stress is the normal stress reduced by the fluid pressure, which tends to open the fracture. The effective normal stress is formally defined as

$$\bar{\sigma}_\mathrm{n} = \sigma_\mathrm{n} - \mathcal{S}P, \tag{45}$$

where $\mathcal{S}$ is the Biot effective stress constant (Biot 1941). Based upon hydromechanical laboratory tests, Duveau *et al.* (1997) defined the Biot effective stress coefficient in terms of the fraction of the fracture in contact, $\mathcal{S} = 1 - S_c$.

A change in the effective stress field acting on the fracture typically leads to a change in the aperture of the fracture, inducing a normal displacement Δa. A simple expression follows from an elastic model of the fracture, which leads to a linear relationship

$$\Delta a = -\frac{\Delta\bar{\sigma}_\mathrm{n}}{k_\mathrm{n}}, \tag{46}$$

where $\Delta\bar{\sigma}_\mathrm{n}$ is the change in the effective normal stress and k_n is the initial normal fracture stiffness (Cappa *et al.* 2008). There are more complicated models for the relationship between aperture changes and the normal stress and pressure changes (Goodman 1974) but we shall not consider them here. Substituting the expression for

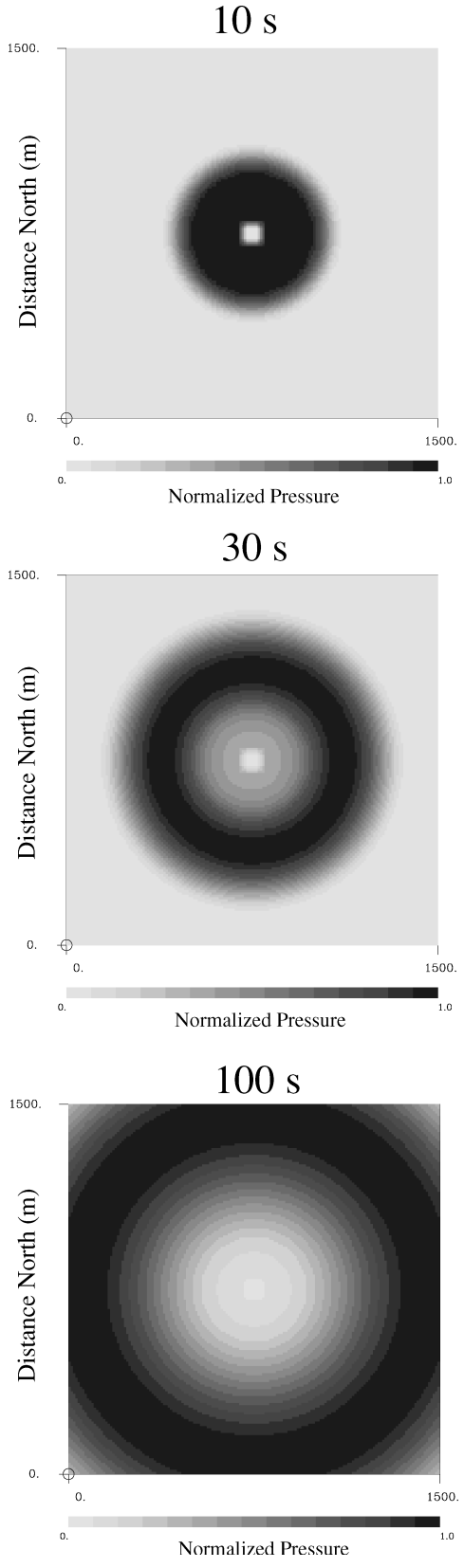

Figure 5. A 2-D view of the self-similar solution in a cylindrical medium. Three snapshots of the normalized pressure variations for propagation of a cylindrical disturbance in the radial direction. The source is an impulse in time, located at the point (750 m, 750 m). The pressure is normalized by the peak value in each node of the grid.

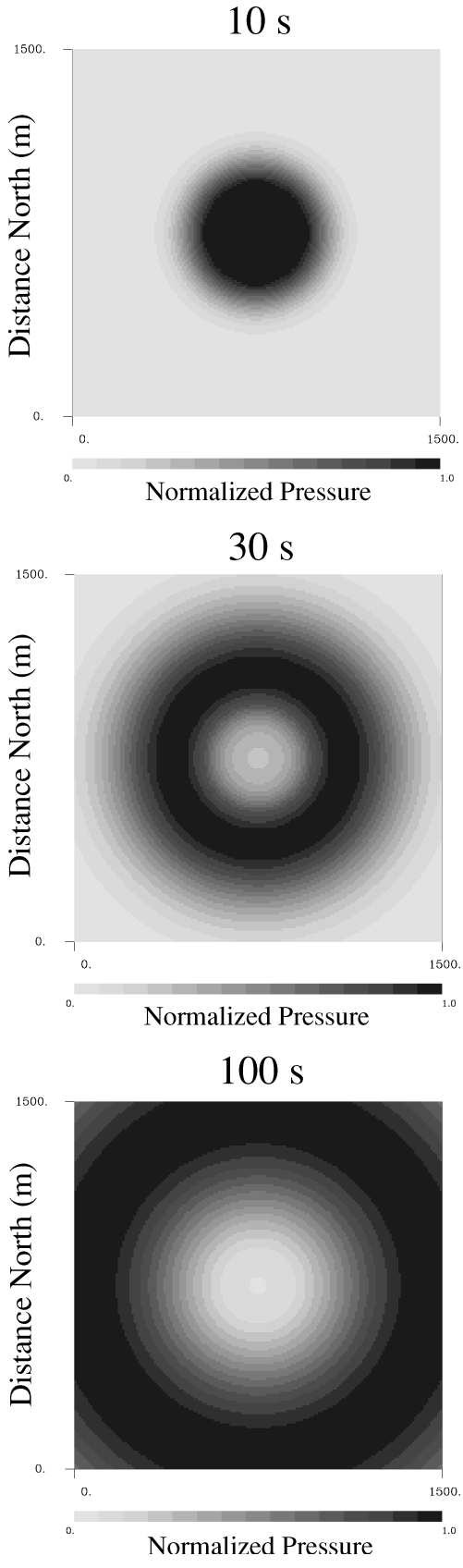

Figure 6. A 2-D view of the asymptotic solution in a cylindrical medium. As in Fig. 5, the source is an impulse, located at the point (750 m, 750 m). The pressure is normalized by the peak value in each node of the grid.

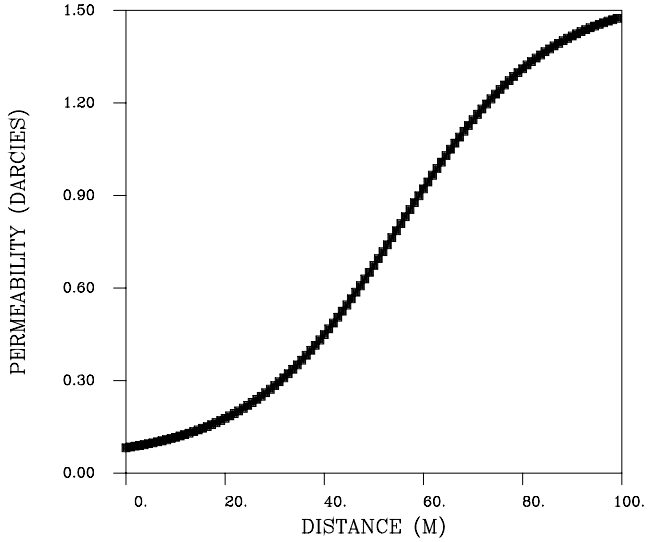

Figure 7. The spatial variation in permeability used in the comparison of the numerical and asymptotic solutions. The permeability increases from values below 0.1 Darcies to values just under 1.5 Darcies according to the function $K_x(x) = \tanh[(x - x_c)/w]$ where $x_c = 55$ m and $w = 33$ m.

effective stress into eq. (46) leads to a relationship between the change in Δa and the change in fluid pressure and normal stress

$$\Delta a = -\frac{\Delta\sigma_{\rm n} - \mathcal{S}\Delta P}{k_{\rm n}}, \tag{47}$$

where $\Delta P = P(\mathbf{X}, T) - P_b(\mathbf{X}, T)$ where $P_b(\mathbf{X}, T)$ is the background pressure field. Similarly, $\Delta\sigma_{\rm n} = \sigma_{\rm n} - \sigma_{nb}$ is the change in effective normal stress. Substituting the expression (47) into eq. (42) gives

$$\mathbf{U} = -\frac{1}{12}\left[a_{\rm i} - \frac{f}{k_{\rm n}}(\Delta\sigma_{\rm n} - \mathcal{S}\Delta P)\right]^2 \frac{\rho g}{\mu}\nabla H. \tag{48}$$

Note that the expression (48) is just Darcy's law written in terms of hydraulic head H,

$$\mathbf{U} = -\frac{k\rho g}{\mu}\nabla H \tag{49}$$

or

$$\mathbf{U} = -\frac{k}{\mu}\left[\nabla P + \rho g\mathbf{z}\right], \tag{50}$$

where

$$k = \frac{1}{12}\left[a_{\rm i} - \frac{f}{k_{\rm n}}(\Delta\sigma_{\rm n} - \mathcal{S}\Delta P)\right]^2 \tag{51}$$

is the intrinsic or specific permeability (de Marsily 1986, p. 60). Allowing the parameters such as the initial aperture, $a_{\rm i}$ and the fracture normal stiffness, $k_{\rm n}$, to vary as functions of $\mathbf{X}$ produces an intrinsic permeability of the form $k(\mathbf{X}, P)$. In what follows we shall assume that the fracture normal stiffness, $k_{\rm n}$, is constant while allowing the initial aperture to be a function of depth, z.

As an aside we note that, for flow in a fracture, the permeability is actually an anisotropic quantity because its value depends strongly on the direction of flow with respect to the plane of the fracture. If the flow restricted to the plane of the fracture is isotropic we can reduce the permeability to a scalar measure by integrating over the direction normal to the fracture plane (de Marsily 1986, p. 72). The resulting quantity, known as the transmissivity, relates the head gradient within the fracture to the flow velocity within the fracture and leads to the well-known cubic law (Witherspoon *et al.* 1980).

Compressibility and the Storage Coefficient

The other important coefficient in the governing pressure eq. (8) is the coefficient C_ρ, defined in eq. (9). Noting the definition of ϕ_ρ we can write the derivative with respect to pressure as

$$C_\rho(\mathbf{x}, P) = \phi\frac{\partial\rho}{\partial P} + \rho\frac{\partial\phi}{\partial P}. \tag{52}$$

For liquid water the isothermal compressibility (de Marsily 1986, p. 102) is rather small, 5.0×10^{-10} Pa^{-1} and for this reason we shall

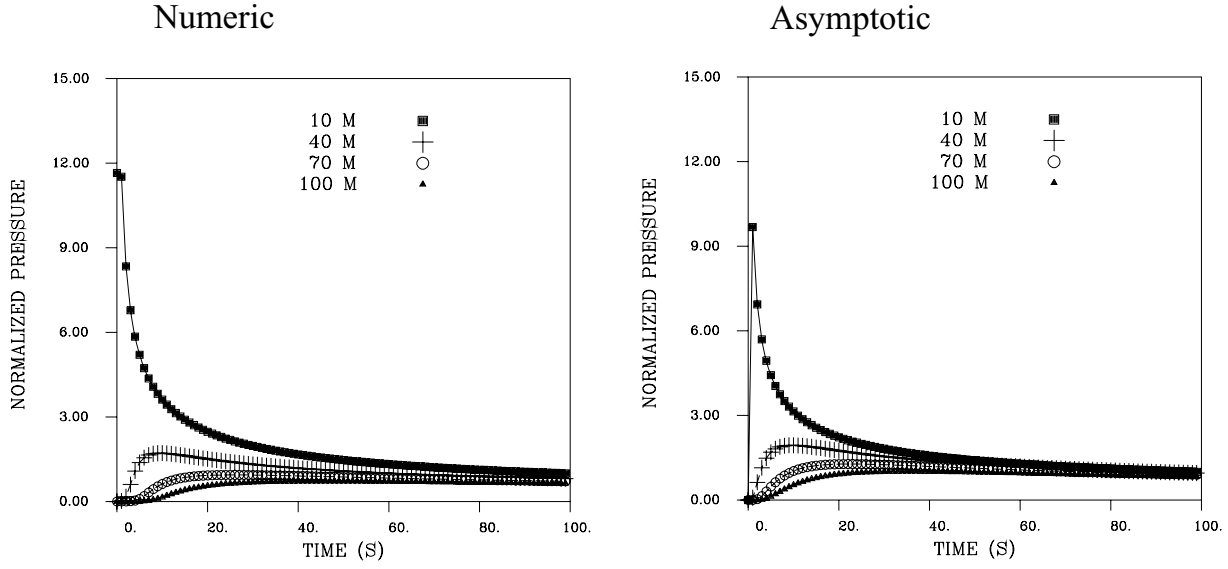

Figure 8. Left-hand panel: the numerical solution corresponding to the spatially-varying permeability shown in Fig. 7. The numerical solution is computed using a finite-element algorithm. Right-hand panel: the asymptotic solution for a medium with the spatially-varying permeability shown in Fig. 7.

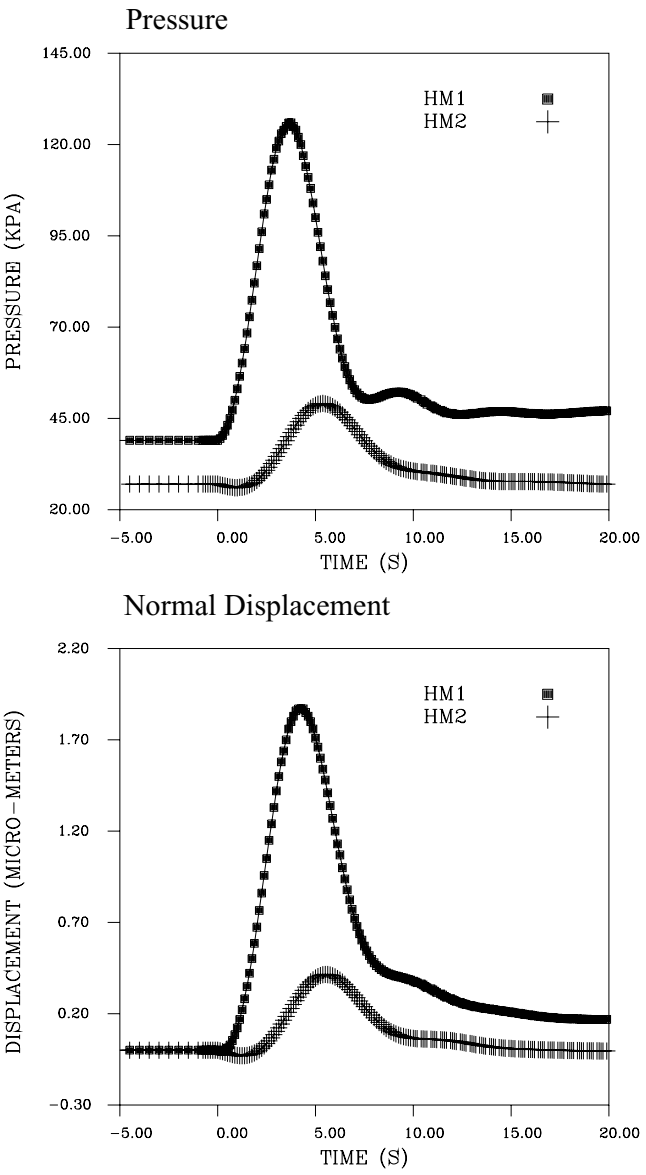

Figure 9. Pressure and normal displacement measurements made at the Coaraze Laboratory site in France. Top panel: pressures measured in boreholes HM1 and HM2, spaced 1 m apart. Bottom panel: normal displacements for the corresponding boreholes.

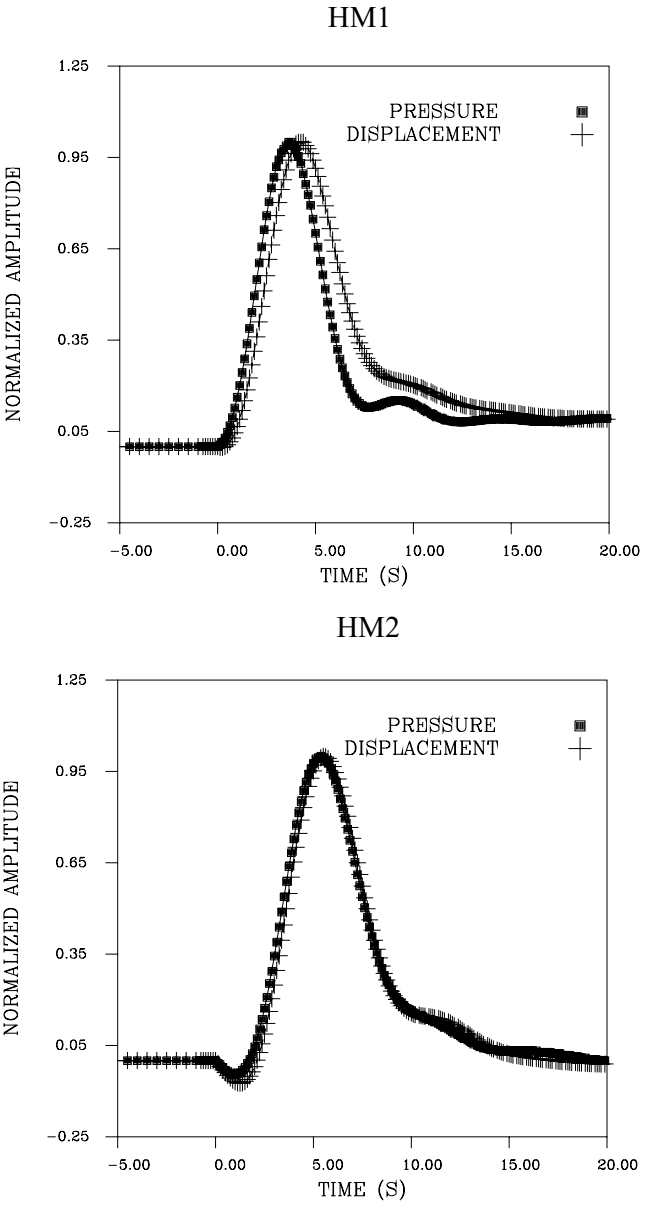

Figure 10. A comparison of pressure and displacement observed in the two boreholes HM1 and HM2. Top panel: normalized pressure superimposed on the normalized displacement curve for the injection borehole HM1. The curves have been normalized such that the peak amplitude is 1. Bottom panel: normalized pressure and displacement for the observation borehole HM2.

assume that the fluid is incompressible. Then, eq. (52) becomes

$$C_\rho(\mathbf{x}, P) = \rho \frac{\partial \phi}{\partial P}. \tag{53}$$

The change in the pore volume is due to the opening of the fracture, the change in aperture and so

$$C_\rho(\mathbf{x}, P) = \frac{\mathcal{A}}{\mathcal{V}} \rho \frac{\partial \Delta a}{\partial P}, \tag{54}$$

where $\mathcal{A}$ is the unit area and $\mathcal{V}$ is the unit volume. Making use of the definition of Δa, eq. (47), and $\Delta P = P - P_b$, we arrive at our final expression for C_ρ

$$C_\rho(\mathbf{x}, P) = -\frac{\rho \mathcal{A} \mathcal{S}}{\mathcal{V} k_{\rm n}}. \tag{55}$$

Thus, under the stated assumptions, the storage coefficient does not depend upon $\mathbf{X}$ or $P(\mathbf{X}, T)$.

3.2.4 Modelling the background pressure field $P_0(\mathbf{X})$ and associated permeability variation

Summarizing up to this point, on the basis of an elastic hydromechanical model of a fluid filled fracture, we have derived an expression for the permeability $k(\mathbf{x}, P)$ which depends upon both the fluid pressure and position within the fracture. This relationship can be used in the asymptotic solution presented in Section 2 and allows us to predict the pressure variation associated with the pulse test. One important aspect of the modelling will be the fact that the background pressure field, $P_0(\mathbf{X})$, varies as a function of position within the fracture. Because the fracture is vertical and the observation borehole HM2 is situated 1 m above the source borehole

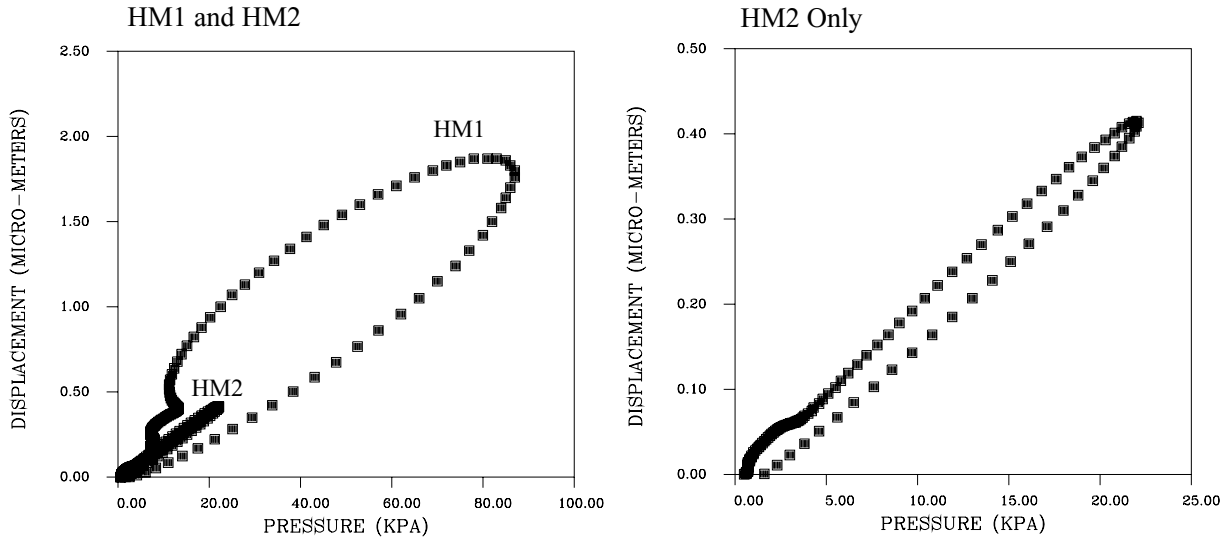

Figure 11. The observed displacement in the borehole plotted against the corresponding observed pressure. The left-most panel displays the displacement and pressure variations observed at both borehole HM1 and borehole HM2. The right-most panel displays the displacement and pressure measured at borehole HM2.

HM1, there is a notable pressure gradient and the pressure at HM2 is significantly lower than the pressure at HM1 (Fig. 9). This will have implications for the propagation of the pressure pulse, for example the traveltime of the pulse, which depends upon $\kappa(\mathbf{X}, P_0)$, as indicated in eq. (30), will vary as a function of depth. Similarly, the amplitude decay away from the source, given by the expression (31) will depend upon the propagation path.

An important consideration in our modelling is that the background pressure satisfies eq. (21). As a starting point we adopt the simplest model for a pressure increase between the source borehole HM1 and the observation borehole, a linear pressure gradient, for the background pressure model

$$P_0(\mathbf{x}) = \mathbf{c} \cdot \mathbf{x} + b, \tag{56}$$

where

$$\mathbf{c} = \nabla P_0(\mathbf{x}). \tag{57}$$

Substituting the form (56) into the governing equation for the background pressure (21) produces the relationship

$$\boldsymbol{\Upsilon}_0 \cdot \mathbf{c} + \lambda_0 \mathbf{c} \cdot \mathbf{c} = 0 \tag{58}$$

which we may write as

$$[\boldsymbol{\Upsilon}_0 \cdot \mathbf{I} + \lambda_0 \mathbf{c} \cdot \mathbf{I}]\, \mathbf{c} = 0. \tag{59}$$

Note that, for non-zero **a** eq. (59) has a solution if

$$\boldsymbol{\Upsilon}_0 = -\lambda_0 \mathbf{c}. \tag{60}$$

Noting the definitions of $\boldsymbol{\Upsilon}_0$, eqs (11) and (22), and λ_0, eqs (12) and (23), we can write (60) as

$$\nabla \ln K_\rho = -\frac{\partial \ln K_\rho}{\partial P}\mathbf{c} \tag{61}$$

or, noting that **c** is a vector in the vertical direction

$$\nabla \ln K_\rho = -c\frac{\partial \ln K_\rho}{\partial P}\hat{\mathbf{z}}, \tag{62}$$

where c denotes the magnitude of the vector **c** and $\hat{\mathbf{z}}$ is a unit vector in the vertical direction. Assuming that the permeability only varies in the vertical direction due to the pressure increase with depth, we can write this equation as

$$\frac{\partial \ln K_\rho}{\partial z} + c\frac{\partial \ln K_\rho}{\partial P} = 0 \tag{63}$$

or, canceling out the $1/K_\rho$ assuming that the permeability never vanishes, and using the fact that $c = |\nabla P_0|$,

$$\frac{\partial K_\rho}{\partial z} + |\nabla P_0|\frac{\partial K_\rho}{\partial P} = 0. \tag{64}$$

In order to make progress on eq. (64) we must make some assumptions regarding the permeability function $K_\rho(\mathbf{X}, P)$. First, the expression (51) is taken as the governing equation for permeability as a function of pressure and position. Second, we assume that the density change of the fluid, the variation of ρ with depth and pressure, can be neglected over the 1 m change in depth. Third, we assume that both the fracture normal stiffness (k_n) and the fracture roughness (f) are constant over the fracture plane. Fourth, we assume that the normal stress on the fracture (σ_n) only varies as a function of depth, due to the increasing weight of the overlying rock and a constant Poisson's ratio. Finally, we assume that the initial fracture aperture, a_i, only varies as a function of depth, due to the variation of the pressure field $P_0(z)$ and σ_n. We take the background fluid pressure field to be P_b, the constant pressure field before the fracture deforms in response to the weight of the fluid. Conceptually, P_b would be the fluid pressure before the fracture is filled with water and would be either zero or the atmospheric pressure at the site. Similarly, we assume a constant background normal stress field $\sigma_{n\mathrm{b}}$, such as the regional stress field, and a new normal stress field, $\sigma_\mathrm{n}(z)$, due to the weight of the overlying rock. The normal stress field is given by the linear increase in stress with depth

$$\sigma_\mathrm{n}(z) = \rho_r g(z - z_t) + \sigma_{\mathrm{n}b}, \tag{65}$$

where ρ_r is the density of the rock and z_t is the position of the surface of the formation. Similarly, the pressure field, which is due to the weight of the overlying water, is given by

$$P(z) = \rho_l g(z - z_t) + P_b, \tag{66}$$

where ρ_l is the density of water.

Starting with the expression (51) for the intrinsic permeability, we can evaluate the partial derivative with respect to the pressure

$$\frac{\partial K_\rho}{\partial P} = \frac{f\mathcal{S}}{6k_{\rm n}}\left\{a_{\rm i} - \frac{f}{k_{\rm n}}[\sigma_{\rm n}(z) - \sigma_{nb}] + \frac{f\mathcal{S}}{k_{\rm n}}[P(z) - P_b]\right\}. \tag{67}$$

We can also take the derivative of eq. (51) with respect to the depth

$$\frac{\partial K_\rho}{\partial z} = \frac{1}{6}\left\{a_{\rm i} - \frac{f}{k_{\rm n}}[\sigma_{\rm n}(z) - \sigma_{nb}] + \frac{f\mathcal{S}}{k_{\rm n}}[P(z) - P_b]\right\} \times \left[\frac{\partial a_{\rm i}}{\partial z} - \frac{f}{k_{\rm n}}\frac{\partial \sigma_{\rm n}}{\partial z} + \frac{f\mathcal{S}}{k_{\rm n}}\frac{\partial P}{\partial z}\right] \tag{68}$$

Substituting expressions (67) and (68) into eq. (64) results in an equation for the initial aperture $a_{\rm i}(z)$

$$\frac{{\rm d}a_{\rm i}}{{\rm d}z} - \frac{f}{k_{\rm n}}\frac{{\rm d}\sigma_{\rm n}}{{\rm d}z} + \frac{f\mathcal{S}}{k_{\rm n}}\frac{{\rm d}P}{{\rm d}z} = -\nabla P_0\frac{f\mathcal{S}}{k_{\rm n}}. \tag{69}$$

The derivatives of $\sigma_{\rm n}$ and P with respect to the depth z may be evaluated using the linear expressions (65) and (66) to arrive at

$$\frac{{\rm d}a_{\rm i}}{{\rm d}z} - \frac{f}{k_{\rm n}}\rho_r g + \frac{f\mathcal{S}}{k_{\rm n}}\rho_l g = -\nabla P_0\frac{f\mathcal{S}}{k_{\rm n}}. \tag{70}$$

This equation for $a_{\rm i}(z)$ may be integrated to recover the linear form

$$a_{\rm i}(z) = a_0 + a_s z \tag{71}$$

for the aperture as a function of depth, where a_0 is a constant of integration and

$$a_s = \frac{fg}{k_{\rm n}}\left(\rho_r - 2\mathcal{S}\rho_l\right). \tag{72}$$

Substituting the linear expression for $a_{\rm i}(z)$, eq. (71), into the permeability function (51) results in

$$k[z, P_0(z)] = \frac{1}{12}\left[a_0 + a_s z - \frac{f}{k_{\rm n}}(\Delta\sigma_{\rm n} - \mathcal{S}\Delta P)\right]^2 \tag{73}$$

which has an explicit dependence on the vertical coordinate z and an implicit dependence through the pressure field.

3.2.5 Modelling the pressure field $P_1(\mathbf{X}, T)$ due to fluid injection at borehole HM1

Now we consider the evolution of the pressure field $P_1(\mathbf{X}, T)$ due to the injection of fluid in borehole HM1. The governing equation is (24) and the semi-analytic solution is given by the expression (35). In the coefficients $\mathbf{\Psi}_1$, Ψ_2 and κ_0, the background pressure field $P_0(\mathbf{X})$ is given by the linear increase with depth (66), as discussed in the previous subsection. The permeability is given by eq. (51), with the background pressure $P_0(z)$. We assume that the change in the normal stress, which is primarily due to the weight of the overlying rock, does not change as the water is injected and thus $\Delta\sigma_{\rm n} = 0$. In addition, $\Delta P = P - P_0(z)$, so that the permeability is given by

$$K(z, P) = \frac{1}{12\mu}\left\{a_0 + a_s z - \frac{f\mathcal{S}}{k_{\rm n}}[P - \rho_l g(z - z_t) - P_b]\right\}^2. \tag{74}$$

In Fig. 12, we plot the logarithm of the permeability as a function of the pressure due to injection and the elevation within the laboratory site. The permeability increases significantly as the surface is approached and as the injection pressure approaches 150 kPa. In

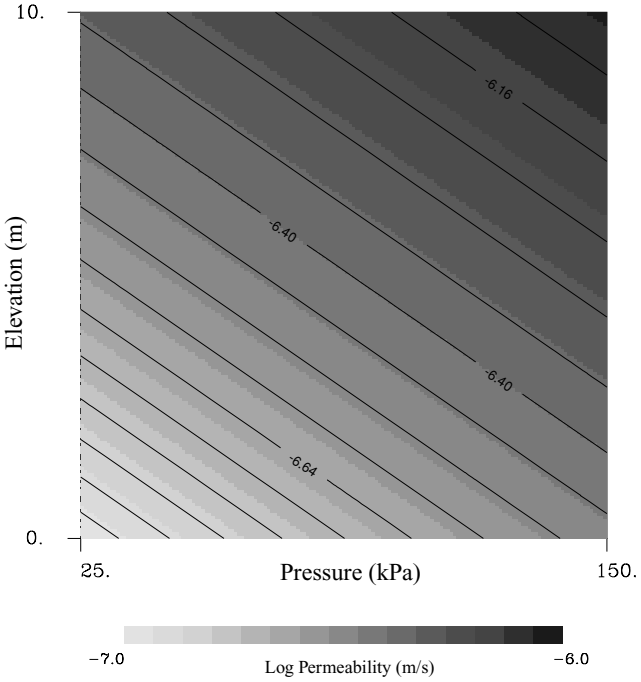

Figure 12. The variation of the logarithm of permeability plotted as a function of the fluid pressure change and the elevation above the base of the limestone outcrop.

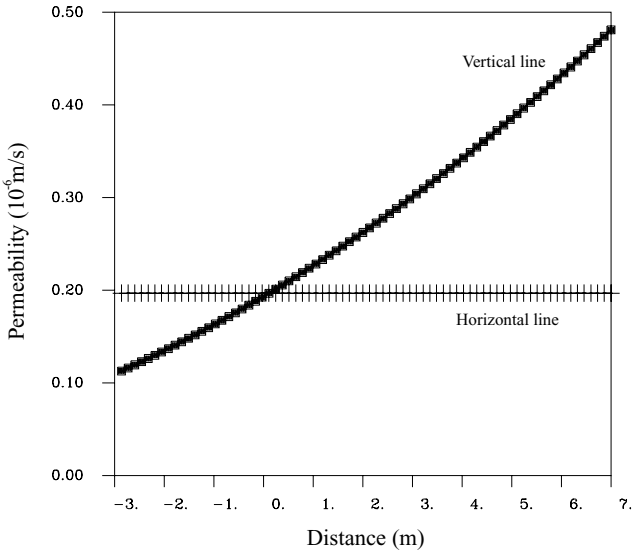

Figure 13. Permeability variation along two lines through the injection well location HM1. One of the traverses is horizontal while the other is vertical.

Fig. 13, we emphasize that the permeability varies with direction in the fracture zone. For example, the permeability changes roughly 500 per cent if one moves from 3 m below the borehole to 7 m above the borehole. Moving laterally by the same amount does not change the permeability. This difference may explain the apparent anisotropy noted by Cappa *et al.* (2008). Those authors required a hydraulic conductivity some 86.3 times greater in the dip direction then that in the strike direction in their modelling of the pulse test results. Such a large variation in permeability with depth is primarily due to the shallow depth of the fracture, less than 10 m. Deeper fractures are overlain by a thick section of rock and the permeability

will not change much as one moves up the fracture by a few metres or a few tens of metres.

In order to predict the response at borehole HM2 due to the injection at HM1 we constructed the full solution given by eq. (35). An important quantity is the 'pseudo-phase' $\sigma(\mathbf{X})$, given by eq. (29) which depends upon the flow properties, as indicated by (30). The depth- and pressure-dependent permeability is given above (74) and the storage coefficient is a constant (55). We emphasize that our modelling involves a number of approximations, for example the fracture stiffness k_n is assumed to be constant, and we are simply trying to capture the overall pressure variation. In particular, we seek to match the arrival time of the pulse, as measured by the time at which the peak pressure is observed at HM2. Furthermore, given the source pulse, we are attempting to match the observed pulse width and general decay.

The parameters used in our modelling are taken from the papers of Cappa *et al.* (2005, 2006, 2008), modified for our fracture aperture model and to match to observed pressure change at HM2 (Fig. 10). The initial fracture aperture at the injection well HM1 was taken to be 1.0×10^{-4} m (Cappa *et al.* 2008). The density of the fluid is assumed to be 1000 kg m^{-3} while that of the limestone is taken to be 2500 kg m^{-3}. The normal stiffness of the fracture, k_n, is set at 8.0 GPa m^{-1} while $\mathcal{S}$ is set at 0.88. The fracture roughness parameter f is set at 2.00 and the Poisson's ratio is assumed to be 0.29. The elevation of the observation interval is inferred from the intersection of the limestone bedding planes with the fault F12 (Cappa *et al.* 2005), 3 m for borehole HM1 and 4 m for borehole HM2. The source pulse was inferred from the pressure response at borehole HM1 and convolved with the predicted response at HM2.

We modified the parameters to account for the fact that our initial aperture and permeability are not uniform over the fracture plane. Rather, the permeability varies as a function of depth. As indicated in eq. (71), the aperture decreases with depth due to the increasing normal stress due to the weight of the overlying rock. Through trial and error we adjusted the normal stiffness (k_n), the Biot effective stress constant ($\mathcal{S}$), and the fracture roughness (f) to match the observed pressure variations. A formal inverse procedure could have been used to fit the observations but that could be the subject of a future investigation. The resulting predicted pressure variation (crosses) at HM2 is shown in Fig. 14, as are the observed pressures (filled squares). Overall, there we are able to match the arrival time of the pressure and the general rise and fall of the pressure as a function of time. We cannot fit some of the detailed pressure variations, such as the pressure decrease just before the arrival of the pressure pulse, and the slight oscillations in the tail of the pulse. These features may be due to non-local pressure and stress propagation and possibly elastic and inertial effects that are not included in our model.

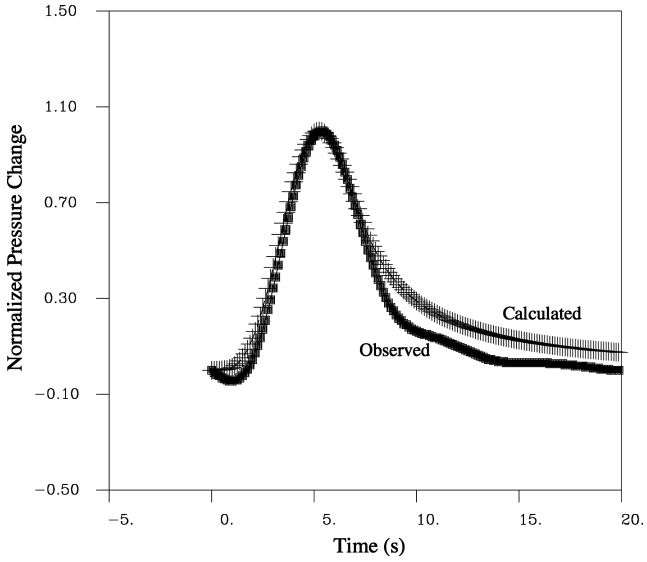

Figure 14. Observed and predicted pressure variation at the observation borehole HM2.

4 DISCUSSION AND CONCLUSIONS

Numerical coupled modelling of fluid flow in a deformable medium is becoming increasingly common (Lewis & Schrefler 1978; Noorishad *et al.* 1992; Rutqvist *et al.* 2002; Minkoff *et al.* 2003). Such modelling is useful as a predictive tool, in exploring the implications of our physical theories, and even for parameter identification and sensitivity studies. However, from the results of a numerical solution it is not always clear how properties of the final solution depend upon the parameters of the medium. The semi-analytic solution presented in this paper should prove useful in both understanding the results of a numerical solution as well as interpreting field data. It was shown that the functional form of the rapidly varying component of the pressure disturbance is similar to the classical solution for the time variation of pressure due to fluid withdrawal from a porous medium (Theis 1935). Also, the expression for the pseudo-phase, which is related to the transient pressure 'arrival time', has a simple relationship to the medium parameters along a trajectory through the model. The trajectory itself indicates the region of sensitivity to the model parameters and proves useful in solving the inverse problem (Vasco *et al.* 2000; Vasco & Finsterle 2004). Similarly, the governing equation for the amplitude indicates that it is sensitive to the geometrical spreading of the trajectories as well as the rate of change of the logarithm of the permeability along the trajectory.

The expression for flow in a medium with pressure-dependent properties should prove useful in interpreting pressure variations induced by fluid injection into fractured rock (Gale 1975; Murphy *et al.* 2004; Cappa *et al.* 2008; Vasco *et al.* 2008) and injection at high pressure. In particular, the expressions for the phase or 'pseudo-phase' amplitude, and the general expression for pressure itself, are similar to those used in the inversion of transient pressure data (Vasco *et al.* 2000; Brauchler *et al.* 2003; He *et al.* 2006; Vasco *et al.* 2008). It should be possible to combine this methodology with the coupled modelling of flow and deformation described in Vasco (2008, 2009). Thus, one could model coupled pressure and deformation in a medium with pressure dependent flow properties. This should be of interest in studying pumping tests in fractures for example. It should also prove valuable in the interpretation of time-lapse seismic studies associated with high production rates and primary production (Hatchell & Bourne 2005; Tura *et al.* 2005; Hawkins *et al.* 2007; Hodgson *et al.* 2007; Rickett *et al.* 2007; Staples *et al.* 2007).

ACKNOWLEDGMENTS

This work was supported by the Assistant Secretary, Office of Basic Energy Sciences of the U. S. Department of Energy under contract DE-AC02-05CH11231. We would like to thank F. Cappa and Y.

Guglielmi for the pressure and displacement data from the pulse test conducted at the Coaraze Laboratory site.

REFERENCES

Anile, A.M., Hunter, J.K., Pantano, P. & Russo, G., 1993. *Ray Methods for Nonlinear Waves in Fluids and Plasmas,* Longman Scientific and Technical, New York.

Audet, D.M. & Fowler, A.C., 1992. A mathematical model for compaction in sedimentary basins, *Geophys. J. Int.,* **110,** 577–590.

Barenblatt, G.I., 1952. On some unsteady motions of a fluid and a gas in a porous medium, *Prikl. Mat. Mekh,* **16,** 67–78 (in Russian).

Bear, J., 1972. *Dynamics of Fluids in Porous Media,* Dover Publications, New York.

Biot, M.A., 1941. General theory of three-dimensional consolidation, *J. appl. Phys.,* **12,** 144–164.

Bluman, G.W. & Cole, J.D., 1974. *Similarity Methods for Differential Equations,* Springer-Verlag, New York.

Booker, J.R. & Carter, J.P., 1986. Analysis of a point sink embedded in a porous elastic half space, *Int. J. Numer. Anal. Methods Geomech.,* **10,** 137–150.

Boussinesq, J., 1868. Memoire sur l'influence des frottements dans les movements reguliers des fluides, *J. Math. Pures Appl.,* **2,** 377–424.

Boussinesq, J., 1904. Recherches theoriques sur l'ecoulement des hoppes d'eau infiltrees dans le sol, *J. Math. Pures Appl.,* **10,** 5–78.

Boyer, R.H., 1961. On some solutions of a non-linear diffusion equation, *J. Math. Phys.,* **40,** 41–45.

Bracewell, R.N., 1978. *The Fourier Transform and Its Applications,* McGraw-Hill Book Company, New York.

Brauchler, R., Liedl, R. & Dietrich, P.. 2003. A travel time based hydraulic tomographic approach, *Water Resour. Res.,* **39,** 20–1-12.

Cappa, F., Guglielmi, Y., Fenart, P., Merrien-Soukatchoff, V. & Thoraval, A., 2005. Hydromechanical interactions in a fractured carbonate reservoir inferred from hydraulic and mechanical measurements, *Int. J. Rock. Mech. Min. Sci.,* **42,** 287–306, doi:10.1016/j.ijrmms.2004.11.006.

Cappa, F., Guglielmi, Y., Rutqvist, J., Tsang, C.-F. & Thoraval, A., 2006. Hydromechanical modelling of pulse tests that measure fluid pressure and fracture normal displacement at the Coaraze Laboratory site, France, *Int. J. Rock. Mech. Min. Sci.,* **43,** 1062–1082, doi:10.1016/j.ijrmms.2006.03.006.

Cappa, F., Guglielmi, Y., Rutqvist, J., Tsang, C.-F. & Thoraval, A., 2008. Estimation of fracture flow parameters through numerical analysis of hydromechanical pressure pulses, *Water Resour. Res.,* **44,** 1–15, doi:10.1029/2008WR007015.

Cohen, J.K. & Lewis, R.M., 1967. A ray method for the asymptotic solution of the diffusion equation, *J. Inst. Math. Appl.,* **3,** 266–290.

Courant, R. & Hilbert, D., 1962. *Methods of Mathematical Physics,* Interscience, New York.

Crank, J., 1975. *The Mathematics of Diffusion,* Oxford University Press, London.

de Marsily, G., 1986. *Quantitative Hydrogeology,* Academic Press, San Diego.

Dean, R., Gai, X., Stone, C. & Minkoff, S., 2006. A comparison of techniques for coupling porous flow and geomechanics, *Soc. Petrol. Eng. J.,* **11,** 132–140.

Duveau, G., Sibai, M., Dunat, X., Skoczylas, F., Henry, J.P., 1997. Modelization du comportement hydromechanique d'un joint rocheux sous contrainte normale, *Revue francaise de geotechnique,* **81,** 41–51.

Fatt, I., 1958. Pore volume compressibilities of sandstone reservoir rocks, *J. Petrol. Tech.,* **10,** 15–16.

Friedlander, F.G. & Keller, J.B., 1955. Asymptotic expansions of solutions of $(\nabla^2 + k^2)\, u = 0$, *Commun. Pure appl. Math.,* **8,** 387.

Gale, J.E., 1975. A Numerical, Field, and Laboratory Study of Flow in Rocks with Deformable Fractures, *PhD thesis*, University of California, Berkeley.

Gilding, B.H. & Peletier, L.A., 1977. On a class of similarity solutions to the porous media equation, *J. Math. Anal. Appl.,* **57,** 522–538.

Goodman, R.E., 1974. The mechanical properties of joints, in *Proceedings of the 3rd International Congress of the International Society of Rock Mechanics*, Denver CO., Vol. 1, pp. 127–140, National Academy of Sciences, Washington, DC.

Grundy, R.E., 1979. Similarity solutions of the nonlinear diffusion equation, *Q. appl. Math.,* **37,** 259–280.

Grundy, R.E., 1983. Large time solution of an inhomogeneous nonlinear diffusion equation *Proc. R. Soc. Lond. A,* **386,** 347–372.

Guglielmi, Y. & Mudry, J., 2001. Quantitative measurements of channel-block hydraulic interactions by experimental saturation of a large, natural, fissured rock mass, *Ground Water,* **39,** 696–701.

Hatchell, P. & Bourne, S., 2005. Rocks under strain: strain-induced time-lapse time shifts are observed for depleting reservoirs, *Leading Edge,* **17,** 1222–1225.

Hawkins, K. *et al.*, 2007. Production-induced stresses from time-lapse time shifts: A geomechanics case study from Franklin and Elgin Fields, *Leading Edge,* **26,** 655–662.

Hayashi, N., Kaikina, E.I., Naumkin, P.I. & Shishmarev, I.A., 2006. *Asymptotics for Dissipative Nonlinear Equations,* Springer-Verlag, Berlin.

He, Z., Datta-Gupta, A. & Vasco, D.W., 2006. Rapid inverse modeling of pressure interference tests using trajectory-based traveltime and amplitude sensitivities, *Water Resour. Res.,* **42,** 1–15.

Hodgson, N., MacBeth, C., Duranti, L., Rickett, J. & Nihei, K., 2007. Inverting for reservoir pressure change using time-lapse time strain: Application to the Genesis Field, Gulf of Mexico, *Leading Edge,* **26,** 649–652.

Jeffrey, A. & Kawahara, T., 1982. *Asymptotic Methods in Nonlinear Wave Theory,* Pitman Advanced Publishing, Boston.

Jones, F.O., 1975. A laboratory study of the effects of confining pressure on fracture flow and storage capacity in carbonate rocks, *J. Petrol. Tech.,* **27,** 21–27.

Kamin, S. & Rosenau, P., 1981. Propagation of thermal waves in an inhomogeneous medium, *Commun. Pure appl. Math.,* **34,** 831–852.

King, J.R., 1993. Exact multidimensional solutions to some nonlinear diffusion equations, *Q. J. Mech. appl. Math.,* **46,** 419–436.

Kline, M. & Kay, I.W., 1965. *Electromagnetic Theory and Geometrical Optics,* John Wiley and Sons, New York.

Korsunsky, S., 1997. *Nonlinear Waves in Dispersive and Dissipative Systems with Coupled Fields,* Addison Wesley Longman, Essex.

Kravtsov, Y.A. & Orlov, Y.I., 1990. *Geometrical Optics of Inhomogeneous Media,* Springer-Verlag, Berlin.

Lacey, A.A., Ockendon, J.R. & Tayler, A.B., 1982. "Waiting-time" solutions of a nonlinear diffusion equation, *SIAM J. appl. Math.,* **42,** 1252–1264.

Lewis, R.W. & Schrefler, B., 1978. A fully coupled consolidation model of the subsidence of Venice, *Water Resour. Res.,* **14,** 223–230.

Leibenzon, L.S., 1947. *Motion of Natural Fluids and Gases in a Porous Medium,* Gostekhizdat, Moscow (in Russian).

Lomize, G.M., 1951. *Flow in Fractured Rocks,* Gosenergoizdat, Moscow (in Russian).

Luneburg, R.K., 1966. *Mathematical Theory of Optics,* University of California Press, Berkeley.

Matsuno, Y., 1991. Similarity solution of a nonlinear diffusion equation describing Alfven wave propagation, *J. Phys. Soc. Japan,* **60,** 3197–3199.

Minkoff, S.E. & Kridler, N.M., 2006. A comparison of adaptive time stepping methods for coupled flow and deformation modeling, *Appl. Math. Modelling,* **30,** 993–1009.

Minkoff, S.E., Stone, C., Bryant, S., Peszynska, M. & Wheeler, M., 2003. Coupled fluid flow and geomechanical deformation modeling, *J. Petrol. Sci. Eng.,* **38,** 37–56.

Minkoff, S.E., Stone, C., Bryant, S. & Peszynska, M., 2004. Coupled geomechanics and flow simulation for time-lapse seismic modeling, *Geophysics,* **69,** 200–211.

Murdoch, L.C. & Germanovich, L.N., 2006. Analysis of a deformable fracture in permeable material, *Int. J. Numer. Anal. Methods Geomech.,* **30,** 529–561.

Murphy, H., Huang, C., Dash, Z., Zyvoloski, G. & White, A., 2004. Semi-analytical solutions for fluid flow in rock joints with pressure-dependent openings, *Water Resour. Res.,* **40,** W12506, doi:10.1029/2004WR003005.

Natale, G. & Salusti, E., 1996. Transient solutions for temperature and pressure waves in fluid-saturated porous rocks, *Geophys. J. Int.,* **124,** 649–656.

Newman, W.I., 1983. Nonlinear diffusion: self-similarity and traveling waves, *Pure appl. Geophys.,* **121,** 417–441.

Noorishad, J., Tsang, C.-F. & Witherspoon, P.A., 1992. Theoretical and field studies of coupled behavior of fractured rocks, 1, Development and verification of a numerical simulator, *Int. J. Rock. Mech. Min. Sci. Geomech. Abstr.,* **29,** 401–409.

Olver, P.J., 1986. *Applications of Lie Groups to Differential Equations,* Springer-Verlag, New York.

Pattle, R.E., 1959. Diffusion from an instantaneous point source with a concentration-dependent coefficient, *Q. J. Mech. appl. Math.,* **12,** 407–409.

Peletier, L.A., 1970. Asymptotic behavior of temperature profiles of a class of non-linear heat conduction problems, *Q. J. Mech. appl. Math.,* **23,** 441–447.

Peletier, L.A., 1971. Asymptotic behavior of solutions of the porous media equation, *SIAM J. appl. Math.,* **21,** 542–551.

Pert, G.J., 1977. A class of similar solutions of the non-linear diffusion equation, *J. Phys. A: Math. Gen.,* **10,** 583–593.

Polubarinova-Kochina, P.Y., 1948. On a non-linear partial differential equation arising in filtration theory, *Dokl. Akad. Nauk SSSR,* **63,** 623–626 (in Russian).

Press, W.H., Teukolsky, S.A., Vetterling, W.T. & Flannery, B.P., 1992. *Numerical Recipes: The Art of Scientific Computing,* Cambridge University Press, Cambridge.

Raghavan, R., Scorer, D.T. & Miller, F.G., 1972. An investigation by numerical methods of the effect of pressure-dependent rock and fluid properties, *Soc. Petrol. Eng. J.,* 267–276.

Rickett, J., Duranti, L., Hudson, T., Regel, B. & Hodgson, N., 2007. 4-D time strain and the seismic signature of geomechanical compaction at Genesis, *Leading Edge,* **26,** 644–647.

Romm, E.S., 1966. *Flow Characteristics of Fractured Rocks,* Nedra, Moscow (in Russian).

Rudnicki, J.W., 1986. Fluid mass sources and point forces in linear elastic diffusive solids, *Mech. Mater.,* **5,** 383–393.

Rutqvist, J., Noorishad, J. & Tsang, C.-F., 1998. Determination of fracture storativity in hard rocks using high-pressure injection testing, *Water Resour. Res.,* **34,** 2551–2560.

Rutqvist, J., Wu, Y.-S., Tsang, C.-F. & Bodvarsson, G., 2002. A modeling approach for analysis of coupled multiphase fluid flow, heat transfer, and deformation in fractures porous rock, *Int. J. Rock. Mech. Min. Sci.,* **39,** 429–442.

Segall, P., 1985. Stress and subsidence resulting from subsurface fluid withdrawal in the epicentral region of the 1983 Coalinga earthquake, *J. geophys. Res.,* **90,** 6801–6816.

Staples, R., Ita, J., Burrell, R. & Nash, R., 2007. Monitoring pressure depletion and improving geomechanical models of the Shearwater Field using 4D seismic, *Leading Edge,* **26,** 636–642.

Terzaghi, K., 1923. Die berechnung der durchlassigkeitsziffer des tones aus dem verlauf der hydrodynamischen spannungserscheinungen, *Sitz. Akad. Wiss.,* **132,** 125–138.

Terzaghi, K. & Peck, R.B., 1967. *Soil Mechanics in Engineering Practices,* John Wiley and Sons, New York.

Theis, C.V., 1935. The relation between the lowering of the piezometric surface and the rate and duration of discharge of a well using groundwater storage, in *Annual Meeting of the American Geophysical Union,* San Francisco, December, pp. 519–524.

Tuck, B., 1976. Some explicit solutions to the non-linear diffusion equation, *J. Phys. D: Appl. Phys.,* **9,** 1559–1569.

Tura, A. *et al.*, 2005. Monitoring primary depletion reservoirs using amplitudes and time shifts from high-repeat seismic surveys, *Leading Edge,* **24,** 1214–1221.

Vasco, D.W., 2008. Modeling quasi-static poroelastic propagation using an asymptotic approach, *Geophys. J. Int.,* **173,** 1119–1135.

Vasco, D.W., 2009. Modelling broad-band poroelastic propagation using an asymptotic approach, *Geophys. J. Int.,* in press, doi:10.1111/j.1365-246X.2009.04263.x.

Vasco, D.W. & Finsterle, S., 2004. Numerical trajectory calculations for the efficient inversion of flow and tracer observations, *Water Resour. Res.,* **40,** W01507, 1–17.

Vasco, D.W., Keers, H. & Karasaki, K., 2000. Estimation of reservoir properties using transient pressure data: an asymptotic approach, *Water Resour. Res.,* **36,** 3447–3465.

Vasco, D.W., Ferretti, A. & Novali, F., 2008. Estimating permeability from quasi-static deformation: temporal variations and arrival-time inversion, *Geophysics,* **73,** O37–O52.

Virieux, J., Flores-Luna, C. & Gibert, D., 1994. Asymptotic theory for diffusive electromagnetic imaging, *Geophys. J. Int.,* **119,** 857–868.

Whitham, G.B., 1974. *Linear and Nonlinear Waves,* John Wiley and Sons, New York.

Witherspoon, P.A., Wang, J.S.Y., Iwai, K. & Gale, J.E., 1980. Validity of the cubic law for fluid flow in a deformable rock fracture, *Water Resour. Res.,* **16,** 1016–1024.

Wu, Y. & Pruess, K., 2000. Integral solutions for transient fluid flow through a porous medium with pressure-dependent permeability, *Int. J. Rock Mech. Min. Sci.,* **37,** 51–61.

Zel'dovich, Y.B. & Kompaneets, A.S., 1950. On the theory of propagation of heat with the heat conductivity depending on temperature, *Collection in honour of the 70th Birthday of Academician A.F. Ioffe, Izdat. Akad. Nauk SSSR Moscow,* pp. 61–71 (in Russian).

APPENDIX A: AN ASYMPTOTIC SOLUTION FOR FLOW IN A MEDIUM WITH SMOOTHLY VARYING PROPERTIES

This appendix sets the stage for solving eq. (16) in a medium with smoothly varying properties. That is, the coefficients $\boldsymbol{\Upsilon}$, λ and κ vary slowly within a particular formation. Note, that there is no limitation on the magnitude of the heterogeneity, just on the spatial-scale of the variation. The technique employed in treating eq. (16) is related to the method of multiple scales or the two-timing method (Whitham 1974; Jeffrey & Kawahara 1982; Anile *et al.* 1993; Korsunsky 1997). We shall modify the technique by not introducing a variable for the phase at this juncture. Rather, one brings in the phase at a later stage, when examining the results in the frequency domain, in Appendix B. For now, we represent the length scale over which the flow properties vary by the variable L. As mentioned above, we are interested in smoothly varying properties, signified by a large value of L. One can only specify the size of L relative to some other physically meaningful quantity. That is, one needs a reference scale with which to compare L and evaluate its size. The scale that makes the most physical sense is the length scale, l, over which the pressure increases from its background value to the value due to pumping or injection. We will model flow in a medium in which the flow properties vary over a spatial scale that is much larger then the distance over which the pressure increases. Thus, we can define a variable ε which is the ratio of the scale-lengths

$$\varepsilon = l/L, \tag{A1}$$

assuming that $\varepsilon \ll 1$, and rescale the problem in terms of ε, defining 'slow' time

$$T = \varepsilon^2 t \tag{A2}$$

and 'slow' space

$$\mathbf{X} = \varepsilon \mathbf{x} \tag{A3}$$

coordinates. The difference in the scaling of the time and space coordinates is necessary to preserve the similarity of the equations, due to the differences in the orders of the time and space derivatives (Cohen & Lewis 1967; Bluman & Cole 1974; Crank 1975). In an asymptotic approach, the pressure is represented as a power series, which may be divergent as $l \rightarrow \infty$, in the ratio ε

$$P(\mathbf{X}, T) = P_0(\mathbf{X}) + \sum_{l=1}^{\infty} \varepsilon^l P_l(\mathbf{X}, T). \tag{A4}$$

An important fact about the series (A4) is that, because $\varepsilon \ll 1$, only the first one or two terms are significant. The coordinate scaling (A2) and (A3) or transformations, lead to changes in the partial derivatives in the governing equation. In particular,

$$\frac{\partial}{\partial t} = \frac{\partial T}{\partial t}\frac{\partial}{\partial T} \tag{A5}$$

and

$$\frac{\partial}{\partial x_i} = \frac{\partial X_i}{\partial x_i}\frac{\partial}{\partial X_i}, \tag{A6}$$

or, using eqs (A2) and (A3),

$$\frac{\partial}{\partial t} = \varepsilon^2 \frac{\partial}{\partial T} \tag{A7}$$

$$\frac{\partial}{\partial x_i} = \varepsilon \frac{\partial}{\partial X_i}. \tag{A8}$$

Furthermore, substituting the power series representation for $P(\mathbf{X}, T)$, eq. (A4), into the coefficients $\boldsymbol{\Upsilon}(\mathbf{X}, P)$, $\kappa(\mathbf{X}, P)$ and $\lambda(\mathbf{X}, P)$ and using a Taylor series expansion of these functions about the background pressure field P_0, gives

$$\boldsymbol{\Upsilon}(\mathbf{X}, P) = \boldsymbol{\Upsilon}(\mathbf{X}, P_0) + \sum_{l=1}^{\infty} \varepsilon^l \frac{\partial^l \boldsymbol{\Upsilon}}{\partial P^l} P_l(\mathbf{X}, T) \tag{A9}$$

$$\kappa(\mathbf{X}, P) = \kappa(\mathbf{X}, P_0) + \sum_{l=1}^{\infty} \varepsilon^l \frac{\partial^l \kappa}{\partial P^l} P_l(\mathbf{X}, T) \tag{A10}$$

$$\lambda(\mathbf{X}, P) = \lambda(\mathbf{X}, P_0) + \sum_{l=1}^{\infty} \varepsilon^l \frac{\partial^l \lambda}{\partial P^l} P_l(\mathbf{X}, T), \tag{A11}$$

where the partial derivatives are evaluated $P = P_0$. Note that we have only expanded the functions to order 1 in P because we are only interested in terms of orders ε^0 and ε^1. Substituting the transformed derivatives and the power series representations of the coefficients into eq. (16) we obtain the expression

$$\begin{aligned}
&\left[\boldsymbol{\Upsilon}(\mathbf{X}, P_0) + \sum_{l=1}^{\infty} \varepsilon^l \frac{\partial^l \boldsymbol{\Upsilon}}{\partial P^l} P_l(\mathbf{X}, T)\right] \cdot \nabla P \\
&\quad + \left[\lambda(\mathbf{X}, P_0) + \sum_{l=1}^{\infty} \varepsilon^l \frac{\partial^l \lambda}{\partial P^l} P_l(\mathbf{X}, T)\right] \nabla P \cdot \nabla P + \nabla \cdot \nabla P \\
&\quad = \left[\kappa(\mathbf{X}, P_0) + \sum_{l=1}^{\infty} \varepsilon^l \frac{\partial^l \kappa}{\partial P^l} P_l(\mathbf{X}, T)\right] \frac{\partial P}{\partial T},
\end{aligned} \tag{A12}$$

where we have factored out ε^2, and the gradients are now evaluated with respect to the slow spatial variables $\mathbf{X}$. Replacing $P(\mathbf{X}, T)$ by the power series representation (A4) results in an equation containing an infinite number of terms, each of a particular order in ε.

APPENDIX B: AN ASYMPTOTIC SOLUTION OF THE EQUATION FOR $P_1(\mathbf{X}, T)$

In this appendix, we utilize an asymptotic expansion in frequency to produce an approximate solution to eq. (24), valid for smoothly varying heterogeneity (Virieux *et al.* 1994; Vasco *et al.* 2000). Because the technique has been described elsewhere and applied to several problems in fluid flow (Brauchler *et al.* 2003; Vasco & Finsterle 2004; He *et al.* 2006), we only outline the method and present the resulting equations.

In order to derive a semi-analytic solution we work in the frequency domain by applying the Fourier transform to eq. (24). The resulting equation is

$$\nabla \cdot \nabla \hat{P}_1 + \boldsymbol{\Psi}_1 \cdot \nabla \hat{P}_1 + \Psi_2 \hat{P}_1 = \mathrm{i}\omega\kappa_0 \hat{P}_1, \tag{B1}$$

where $\hat{P}_1(\mathbf{X}, \omega)$ is the Fourier transform of $P_1(\mathbf{X}, T)$ (Bracewell 1978) and

$$\boldsymbol{\Psi}_1 = \boldsymbol{\Upsilon}_0 + 2\lambda_0 \nabla P_0, \tag{B2}$$

$$\Psi_2 = \frac{\partial \boldsymbol{\Upsilon}_0}{\partial P} \cdot \nabla P_0 + \frac{\partial \lambda_0}{\partial P} \nabla P_0 \cdot \nabla P_0, \tag{B3}$$

and

$$\kappa_0 = \kappa(\mathbf{X}, P_0) = \frac{C_\rho}{K_\rho}. \tag{B4}$$

Because we are interested in the rapidly-varying component of pressure, rather than the slower variations, consider a solution in the form of a power series in $1/\sqrt{\omega}$

$$\hat{P}_1(\mathbf{X}, \omega) = \mathrm{e}^{-\sqrt{-\mathrm{i}\omega}\sigma(\mathbf{X})} \sum_{n=0}^{\infty} \frac{A_n(\mathbf{X})}{(\sqrt{-\mathrm{i}\omega})^n}. \tag{B5}$$

For the high-frequency component of $P(\mathbf{X}, \omega)$, for large ω, the first few terms of (B5) are the most important. For example, in many cases the zeroth-order term,

$$\hat{P}_1(\mathbf{X}, \omega) = A_0(\mathbf{X}) \mathrm{e}^{-\sqrt{-\mathrm{i}\omega}\sigma(\mathbf{X})} \tag{B6}$$

is sufficient to represent the pressure variation (Virieux *et al.* 1994). Taking the inverse Fourier transform with respect to ω produces the time domain equivalent of eq. (B6)

$$P_1(\mathbf{X}, T) = A_0(\mathbf{X})\sigma(\mathbf{X}) \frac{\mathrm{e}^{-\sigma^2(\mathbf{X})/4T}}{2\sqrt{\pi T^3}} \tag{B7}$$

(Virieux *et al.* 1994). Returning to the full expansion, substitute eq. (B5) into the governing eq. (B1) and apply the differential operators ∇ and $\partial/\partial T$ term-by-term. The resulting equation is an endless string of terms, each of a particular order in $1/\sqrt{\omega}$. Because we are interested in the high-frequency component of the pressure change, the frequency ω is assumed to be large. Thus, only the terms in the lowest power of $1/\sqrt{\omega}$ are considered to be significant. The following two subsections consider terms of lowest order in $1/\sqrt{\omega}$: those of order $(1/\sqrt{\omega})^{-2} \sim \omega$ and $(1/\sqrt{\omega})^{-1} \sim \sqrt{\omega}$.

B1 Terms of order ω: a governing equation for $\sigma(\mathbf{X})$

Retaining terms of lowest order in $1/\sqrt{\omega}$ results in a non-linear differential equation for the function $\sigma(\mathbf{X})$ (Vasco *et al.* 2000)

$$\nabla\sigma \cdot \nabla\sigma = \kappa_0, \tag{B8}$$

the equivalent of the Eikonal equation in hyperbolic wave propagation (Friedlander & Keller 1955; Kravtsov & Orlov 1990; Anile

et al. 1993). A physical interpretation of $\sigma(\mathbf{X})$ may be obtained from the time-domain equivalent of the zeroth-order solution, eq. (B7). As shown by Virieux *et al.* (1994), differentiating the expression (B7) with respect to time and setting the resulting equation to zero, We find that

$$\sigma(\mathbf{X}) = \sqrt{6T_{\text{peak}}}, \tag{B9}$$

where T_{peak} is the time associated with the occurrence of the peak pressure at the location $\mathbf{X}$. Thus, $\sigma(\mathbf{X})$ is related to the 'arrival time' of the peak amplitude of $P_1(\mathbf{X}, T)$.

There is a well established link between the differential equation (B8) and its bi-characteristic equations, a set of ordinary differential eqs (Courant & Hilbert 1962) for the coordinates of a path $\mathbf{X}(s)$ through the model and $\sigma[\mathbf{X}(s)]$, where s is the distance along the path. The bi-characteristic equations for $\mathbf{X}(s)$ and $\sigma[\mathbf{X}(s)]$ are

$$\frac{\mathrm{d}\mathbf{X}}{\mathrm{d}s} = \frac{\mathbf{p}}{\varsigma} \tag{B10}$$

$$\frac{\mathrm{d}\mathbf{p}}{\mathrm{d}s} = \nabla\varsigma, \tag{B11}$$

where $\mathbf{p} = \nabla\sigma$ and

$$\varsigma = \sqrt{\kappa_0}. \tag{B12}$$

These equations can either be solved using a numerical technique, such as a shooting method coupled with a Newton-Raphson algorithm (Press *et al.* 1992), or using the results of a numerical simulator to compute $\sigma(\mathbf{X})$ and subsequently $\mathbf{p}$ (Vasco & Finsterle 2004). Writing eq. (B8) in a coordinate system oriented along the trajectories $\mathbf{X}(s)$, taking the square root, and integrating gives

$$\sigma(\mathbf{X}) = \int_{\mathbf{X}} \sqrt{\kappa_0}\mathrm{d}s, \tag{B13}$$

an equation relating the 'phase' or 'pseudo-phase' to the flow properties, as contained in κ_0 [see eq. (B4)].

B2 Terms of order $\sqrt{\omega}$: a governing equation for $A_0(\mathbf{X})$

Consideration of terms of order $\sqrt{\omega}$ results in an equation for the zeroth-order amplitude, $A_0(\mathbf{X})$,

$$2\nabla\sigma \cdot \nabla A_0 + (\nabla \cdot \nabla\sigma + \boldsymbol{\Psi}_1 \cdot \nabla\sigma)\, A_0 = 0 \tag{B14}$$

because $\sigma(\mathbf{X})$ is known through the solution of eq. (B8). For a medium in which the conductivity and background pressure are constant, Ψ_1 vanishes and eq. (B14) reduces to the standard transport equation treated in geometrical optics (Kline & Kay 1965; Kravtsov & Orlov 1990). Introducing the variable γ such that

$$\mathrm{d}\gamma = \frac{\mathrm{d}s}{\sqrt{\kappa_b}} \tag{B15}$$

eq. (B14) can be written as an ordinary differential equation along the trajectory $\mathbf{X}(s)$

$$2\frac{\mathrm{d}\ln A_0}{\mathrm{d}\gamma} + \frac{\mathrm{d}\ln K}{\mathrm{d}\gamma} + 2\lambda\frac{\mathrm{d}P_0}{\mathrm{d}\gamma} + \nabla \cdot \nabla\sigma = 0 \tag{B16}$$

(Vasco *et al.* 2000). Making use of the Eikonal eq. (B8), the final term in eq. (B16) can be written as

$$\nabla \cdot \nabla\sigma = \frac{\mathrm{d}\ln\sqrt{\kappa_0}J(\gamma)}{\mathrm{d}\gamma}, \tag{B17}$$

where $J(\gamma)$ is the Jacobian which measures the divergence of the trajectories as a function of distance along the trajectory. Substituting (B17) into eq. (B16) and integrating provides an equation describing the evolution of the amplitude along the trajectory $\mathbf{X}(\gamma)$

$$A_0(\gamma) = A_0(\gamma_0)\sqrt{\frac{K_x(\gamma_0)}{K_x(\gamma)}}\sqrt{\frac{\sqrt{\kappa_0(\gamma_0)}J(\gamma_0)}{\sqrt{\kappa_0(\gamma)}J(\gamma)}}\,\frac{\mathrm{e}^{-\eta(\gamma_0)}}{\mathrm{e}^{-\eta(\gamma)}}, \tag{B18}$$

where

$$\eta(\gamma) = \int_0^{\gamma} \lambda\frac{\mathrm{d}P_0}{\mathrm{d}\gamma'}\mathrm{d}\gamma' \tag{B19}$$

(Vasco *et al.* 2000).